

A SEARCH FOR H I IN FIVE ELLIPTICALS WITH FINE STRUCTURE

J. E. HIBBARD

National Radio Astronomy Observatory, 520 Edgemont Road, Charlottesville, VA, 22903; jhibbard@nrao.edu

A. E. SANSOM

Centre for Astrophysics, University of Central Lancashire, Preston PR1 2HE, UK; AESansom@uclan.ac.uk

To Appear in the February 2003 AJ

ABSTRACT

We report on VLA H I spectral line observations of five early-type galaxies classified as optically peculiar due to the presence of jets, ripples or other optical “fine structure”. We detect H I within the primary beam (30' HPBW) in four of the five systems. However, in only one case is this gas associated with the targeted elliptical galaxy. In the other cases the H I is associated with a nearby gas-rich disk or dwarf galaxy. The one H I detection is for NGC 7626, where we tentatively detect an H I cloud lying between 20 and 40 kpc southwest of the galaxy center. Its origin is unclear. Our failure to detect obvious tidal H I features suggests that if these fine-structure ellipticals are remnants of disk galaxy mergers, either the progenitors were gas poor, or they are well evolved and any gaseous tidal features have dispersed and/or been converted into other phases. Our targeted systems all reside in groups or clusters, and it seems likely that tidal H I is shorter lived in these environments than suggested by studies of more isolated merger remnants.

Subject headings: galaxies: individual (NGC 3610, NGC 3640, NGC 4382, NGC 5322, NGC 7626) — galaxies: interactions — galaxies: ISM — galaxies: peculiar

1. INTRODUCTION

It was once believed that elliptical galaxies were evolved objects with simple morphologies. However, early image processing techniques revealed that anywhere from one-fourth to one-third of such galaxies exhibit faint morphological peculiarities in the form of shells, ripples, and extended plumes (Malin 1978, 1979; Malin & Carter 1980, 1983; Schweizer & Ford 1984; Schweizer & Seitzer 1988, 1992 hereafter SS92; Reid, Boisson & Sansom 1994). Numerical work soon demonstrated that such features could be reproduced either by small accretion events (Quinn 1984; Dupraz & Combes 1986; Hernquist & Quinn 1988, 1989) or by major mergers (Hernquist & Spergel 1992; Hibbard & Mihos 1995). The appearance of such features in heretofore “normal” ellipticals is seen as strong support for the Toomre merger hypothesis that (some) elliptical galaxies evolve from the merger of disk galaxies (Toomre & Toomre 1972, Toomre 1977).

In an effort to quantify the frequency and quantity of such morphological peculiarities, Schweizer et al. (1990) introduced a “fine-structure index”, Σ , which increases with the amount of morphological peculiarities (for detailed review, see Schweizer 1998). Statistically, galaxies with larger values of Σ have observational characteristics (colors and spectral-line strengths) consistent with the presence of younger stellar populations, supporting the idea that they represent more recent mergers in which star-

bursts have occurred (Schweizer et al. 1990; SS92). This association suggests that the fine-structure index might provide a means to locate evolved merger remnants lying in the so-called “King Gap” between ~ 1 Gyr old remnants and old ellipticals (I. King, quoted in Toomre 1977).

However, some recent studies have called into question the identification of ellipticals with large amounts of fine structure as aged merger remnants (Silva & Bothun 1998a, 1998b). Since such subtle morphological peculiarities may arise from less structurally damaging events, such as accretions, they are not unambiguous signatures of major mergers. To remove this ambiguity, it is desirable to find a more direct link between a high fine-structure index and a merger origin.

Some clues as to the expected appearance of “King Gap” objects are provided by observations of nearby systems which are undeniably the remnants of disk-disk mergers. The best examples of such objects are the last two members of the “Toomre Sequence” (Toomre 1977), a proposed evolutionary sequence of disk-disk mergers. These two systems, NGC 3921 and NGC 7252, are evolved merger remnants with single nuclei, post-burst stellar populations, relaxed $r^{1/4}$ light profiles, and with dynamical ages of ~ 0.5 – 1 Gyr (Schweizer 1982, 1996, Schweizer et al. 1996, Hibbard & Mihos 1995, Miller et al. 1997, Hibbard & Yun 1999). H I mapping of these systems with the VLA¹ shows their tidal tails to be rich in atomic hydrogen (Hibbard et al. 1994, Hibbard & van Gorkom 1996) firmly establishing

¹The VLA of the National Radio Astronomy Observatory is operated by Associated Universities, Inc., under cooperative agreement with the National Science Foundation.

their status as disk-merger products.

Both remnants are also found to have a very low central HI content. This result is somewhat surprising, not only in view of large amounts of HI which must have been sent into the central regions during the early stages of merging (e.g. Barnes & Hernquist 1991), but also in view of the atomic gas-rich material that is observed streaming back into the remnant bodies from the tidal tails (Hibbard & Mihos 1995, Yun & Hibbard 2001). These studies suggest that as the merger evolves, the remnant should have a decreasing amount of fine structure, decreasing amounts of both inner and outer tidal gas, and a multi-epoch aging stellar population.

The present study is an attempt to locate products of gas-rich mergers intermediate in age between recent merger remnants like NGC 3921 & NGC 7252 and ellipticals with less obvious peculiarities. HI mapping of morphologically peculiar early type galaxies provides strong evidence pointing to a gas-rich merger origin for a number of objects (e.g. Schiminovich et al. 1994, 1995; Lim & Ho 1999; Balcells et al. 2001; Chang et al. 2001). With this in mind, we have targeted five ellipticals with varying amounts of optical fine structure ($\Sigma = 2.0 - 7.6$) for HI mapping observations with the VLA in its most compact configuration (D-array) to look for the remnants of gas-rich tidal features in the outer regions. The five systems are NGC 3610, NGC 3640, NGC 4382, NGC 5322 and NGC 7626. In this paper we report the results of the HI observations of these five galaxies.

The present paper is structured as follows. In §2 we describe the selection criterion used to define the targets for this study. §3 we describe the VLA observations and data reduction. In §4 we describe the results for each of the five systems, and in §5 we discuss these results. Finally we summarize our conclusions in §6.

2. SAMPLE SELECTION

The galaxies for this study were chosen from the sample of 69 field elliptical and S0 galaxies for which the fine-structure index has been tabulated by SS92. The fine-structure index is defined as $\Sigma = S + \log(1+n) + J + B + X$, where S is a visual estimate of the strength of the most prominent ripples, n is the number of detected ripples, J is the number of luminous plumes or “jets”, B is a visual estimate of the maximum boxiness of isophotes, and X indicates the absence or presence of an X-structure. The well known young ($\sim 0.5-1$ Gyr) merger remnants NGC 3921 and NGC 7252 have $\Sigma = 8.8$ and 10.1 , respectively, while the sample of field S0’s and Ellipticals studied by SS92 have values in the range $\Sigma = 0 - 7.6$.

The five galaxies chosen for this study are listed in Table 1, along with their basic properties, group membership, fine-structure index, and observational details. We selected the three galaxies in the list of SS92 with the highest values of Σ (NGC 3610, NGC 3640, NGC 4382). We originally chose galaxies to also cover a range of X-ray excess (L_X/L_B), so that we might address whether merger remnants “grow” X-ray halos as tidal gas falls back towards

the remnant (Hibbard et al. 1994, Fabbiano & Schweizer 1995, Read & Ponman 1998). However, a re-analysis of the ROSAT X-ray data for these systems (Sansom, Hibbard & Schweizer 2000) shows that all but NGC 7626 are in the lowest X-ray class, so we will not address this question here. In an earlier study (Sansom, Hibbard & Schweizer 2000), we used the present sample along with the early-type galaxies in the list of SS92 that have existing X-ray observations, to test the hypothesis that X-ray halos form as cold tidal gas falls back into the remnant bodies. We found no clear trends, other than the previously reported trend for recent merger remnants to be X-ray faint (Fabbiano & Schweizer 1995; Georgakakis, Forbes & Norris 2000; O’Sullivan, Forbes & Ponman 2001).

3. VLA DATA

The neutral hydrogen data were collected in December of 1997 using the VLA in its spectral line mapping mode. The array was in its most compact D-array configuration, providing maximum sensitivity to extended emission. Five galaxies and several calibrators were observed. Table 1 gives a log of these observations.

Since the atomic gas within tidal debris typically has narrow linewidths ($\sigma_v \sim 5-10$ km s⁻¹; Hibbard et al. 1994, Hibbard & van Gorkom 1996), the correlator mode was chosen to give the smallest channel spacing while still covering the expected range of velocities for tidal gas. We therefore chose the 2AC mode with on-line Hanning smoothing and a 3.125 MHz bandwidth, resulting in 63 spectral channels each of width ~ 10.4 km s⁻¹ and a total velocity coverage of ~ 650 km s⁻¹. This is sufficient to cover the spread of velocities observed in other peculiar ellipticals (~ 500 km s⁻¹, e.g. Schiminovich et al. 1994, 1995, 2001). However, most of the target ellipticals are members of loose groups or clusters (cf. §4) and the present observations do not cover the velocity range of all group/cluster members. The field-of-view is set by the 25m diameter of the individual array elements, and amounts to a half-power beam width (HPBW) of 30’. Our on-source integration time of ~ 2 hours per source provides an rms noise of ~ 0.6 mJy/beam, corresponding to a 3σ column density sensitivity of $\sim 7 \times 10^{18}$ cm⁻² per channel over a typical beam size of 60’’ \times 50’’ (see Table 1).

The data were reduced using the AIPS software. For each observation the absolute flux level was set by observing a standard VLA flux calibrator. The antenna phases were calibrated with observations of an unresolved continuum source before and after each galaxy observation. The bandpass was calibrated using either the flux or phase calibrator, whichever provided the highest signal to noise. For details on VLA observation and calibration techniques, see Taylor, Carilli & Perley (1999). For the specifics of spectral line data reduction and imaging, see Rupen (1999).

The spectral response of the VLA resulted in 55 usable channels (channels 3-57) out of the 63 channel datacubes. The continuum was removed using an iterative procedure which involved subtracting linear fits to the visibilities at either end of the passband. Various combinations of chan-

nels were used in the fit, and the resulting datacube was mapped and reviewed to determine the range of line-free channels. In cases where HI was detected from a companion at velocities significantly different from the central velocity setting, separate datacubes were made using the appropriate line-free channels for continuum subtraction.

The data were mapped using a “Robust” weighting parameter of +1 (Briggs 1995), which provides good sensitivity to faint extended emission. Continuum intensity and continuum-subtracted line maps were made of the entire primary beam. The line maps were cleaned using the standard methods in AIPS. To further increase our sensitivity, we smoothed the data first in velocity by a factor of four, then spatially by convolving to a resolution of $90''$. No further detections were made in either of the smoothed datasets and all figures presented here use the full resolution datacubes.

Neutral hydrogen masses are calculated according to the equation $M_{HI} = (2.36 \times 10^5) \times D_{\text{Mpc}}^2 \times \int S_{HI} dv$, where D_{Mpc} is the distance to the source in Mpc, S_{HI} is the continuum subtracted HI line specific intensity in Janskys, v is the velocity expressed in km s^{-1} . The integral is over the line, assuming the atomic gas to be optically thin. M_{HI} is then in units of M_{\odot} per beam. Where no detections were made, six sigma upper limits were estimated from the velocity smoothed datacube (i.e. over an HI linewidth of 42 km s^{-1}). HI masses or mass limits for each of the targets are listed in Table 2. Previous limits for these galaxies were typically $10^8 - 10^9 M_{\odot}$ from single dish observations (Roberts et al. 1991). Limits from our VLA data are typically an order of magnitude lower.

4. RESULTS

In this section we summarize the properties of the observed galaxies and the results of the VLA observations. Galaxy classifications are from the RC3 (de Vaucouleurs et al. 1991), and distances are taken from the *Nearby Galaxy Catalog* (Tully 1988), which adopts $H_0 = 75 \text{ km s}^{-1} \text{ Mpc}^{-1}$. Group assignment was assessed using the Loose Galaxy Groups catalog (Garcia 1993, hereafter LGG), and the number of group members was evaluated via the NASA Extragalactic Database (NED). This information is summarized in Table 1.

We review the morphological properties of each system, listing the values for the fine-structure index and the “heuristic merger age”, as tabulated by SS92. The heuristic merger age was calculated by matching a simple two-burst model of evolving stellar populations to the observed *UBV* colors (see SS92 for details). We also report spectroscopically determined age estimates available from the literature. In most cases, these are derived from Single Stellar Populations (SSP) model fits to four or more spectroscopically derived metallicity- and age-dependent line indices (see e.g. Gonzales 1993, Worthey 1994), and represent a luminosity-weighted mean age for the central stellar population. We briefly describe the results of previous HI observations (culled from the compilations of Huchtmeier & Richter 1989 and Martin 1998). We note that our

VLA observations are most sensitive to narrow HI lines, and may miss HI emission spread over a broad range of velocity. For such emission the large-beam single dish limits are still relevant.

Finally, we present the results of our VLA HI mapping observations, which are summarized in Table 2. Figure 1 shows the integrated HI line maps for each of our five target galaxies contoured upon a greyscale representation of the optical light, taken from the Digital Sky Surveys (DSS). No HI was detected from within the optical bodies of any of the target galaxies. Only NGC 7626 shows evidence of some associated HI, out at projected radii from $\sim 1.5 - 3$ arcmin from the galaxy centre.

4.1. NGC 3610 = UGC 6319

NGC 3610 is a member of the NGC 3642 group (LGG 234), with five cataloged members. The NGC 3642 group itself is a sub-group of the rich (N=170) group No. 94 of Geller & Huchra (1983). The optical velocity from the Updated Zwicky Catalog (Falco et al. 1999) is 1696 km s^{-1} , whereas the HI observations were centered at the old RC3 value of 1787 km s^{-1} . This will not effect our detection sensitivity, since this difference is well within the observed band.

NGC 3610 has the highest value of Σ of any of the early types in the SS92 sample ($\Sigma=7.60$, heuristic merger age 4–7 Gyr). Only the young merger remnants NGC 3921 and NGC 7252 have higher values ($\Sigma=8.8$ and 10.1 , respectively). The optical peculiarities include two or three shells, a central ‘X’-structure, plumes, and extraordinarily boxy outer isophotes (Forbes & Thomson 1992, Whitmore et al. 1997). While the outer isophotes are boxy, the inner isophotes are disk-like, due to an inner disk embedded within its spheroid (Scorza & Bender 1990). The system as a whole is rotationally flattened ($V/\sigma = 1$; Scorza & Bender 1990), and the inner disk is kinematically distinct, with $V/\sigma = 4.5$ (Rix & White 1992). There is no color differences between the main body and the inner disk, and both seem to be comprised of stars with similar ages (Scorza & Bender 1990; Whitmore et al. 1997). These observations are seen as evidence for an accretion, rather than a merger, origin (Scorza & Bender 1990, Silva & Bothun 1998b). However, the presence of an intermediate aged centrally concentrated globular cluster population (Whitmore et al. 1997, 2002) suggests a merger origin. The age of the red, metal rich globular cluster population is consistent with the broadband near-IR and optical age estimates of $\sim 4-7$ Gyr (Silva & Bothun 1998b, SS92).

Previous single dish HI observations of NGC 3610 were conducted by Bieging (1978), who set a 3-sigma upper limit of $\int S_{HI} dv < 2.4 \text{ Jy km s}^{-1}$ using the Effelsberg 100-m telescope ($8'$ HPBW). This places a limit on the HI mass to *B*-band luminosity of $M_{HI}/L_B < 0.012 M_{\odot} L_{\odot}^{-1}$. We find no HI emission within the primary beam of the VLA observations. The new HI limit is over an order of magnitude lower than the previous limit ($M_{HI}/L_B < 4 \times 10^{-4} M_{\odot} L_{\odot}^{-1}$). None of the other members of the LGG 234 group fall within the primary beam ($30'$ HPBW, or

130 kpc radius at the adopted distance of 29.2 Mpc) and velocity coverage of the present HI observations.

4.2. *NGC 3640 = UGC 6368*

NGC 3640 is a member of NGC 3640 group (LGG 233), with seven cataloged members. However, none of the other group members fall within the primary beam (105 kpc radius at the adopted distance of 24.2 Mpc) and velocity coverage of the present HI observations. The E pec galaxy NGC 3641 lies just 2.9' south of NGC 3640, but its velocity ($V_{\odot}=1755 \text{ km s}^{-1}$) lies outside the observed band.

Along with NGC 4382, NGC 3640 has the second highest value of the fine-structure index in the SS92 compilation ($\Sigma=6.85$, heuristic merger age 6–8 Gyr). It has a number of morphological peculiarities, including shells, boxy isophotes, a minor-axis dust lane, and like NGC 3610 it is a fast rotator ($V/\sigma=1.5$; Prugniel et al. 1988). The second generation blue DSS image shows what appears to be a faint tidal tail extending directly to the north by about 10' (see Fig. 1). Prugniel et al. (1988) argue that NGC 3640 is a merger in progress, probably with a gas-poor system. Both the heuristic merger age derived by SS92 and the near-IR colors of NGC 3640 argue against a major starburst having occurred within the previous 3 Gyr (Silva & Bothun 1998a, 1998b).

NGC 3640 was previously searched for HI by Shostak et al. (1975), who set an upper limit of $\int S_{\text{HI}} dv < 2.9 \text{ Jy km s}^{-1}$ using the NRAO 300 ft telescope (9.3' HPBW), and by Lake & Schommer (1984), who set an upper limit of $\int S_{\text{HI}} dv < 0.6 \text{ Jy km s}^{-1}$ using the 305-m dish at Arecibo (3.3' HPBW). This places a limit on the HI mass to B-band luminosity of $M_{\text{HI}}/L_B < 0.003 M_{\odot} L_{\odot}^{-1}$.

We detect no HI emission associated with NGC 3640 ($M_{\text{HI}}/L_B < 6 \times 10^{-4} M_{\odot} L_{\odot}^{-1}$). While none of the other members of the LGG 233 group fall within our VLA settings, we do detect HI in an uncataloged galaxy lying 15.1' (105 kpc) to northeast at 11:21:51.5 +03:24:17 (J2000). The integrated HI emission is contoured on the DSS image in Fig. 1, and the HI channel maps of the emission are given in Figure 2. From the DSS image, the companion appears to be a highly-inclined low surface brightness dwarf spiral, and the HI kinematics are characteristic of regular disk rotation. The total detected HI flux, after correction by primary beam attenuation, is 2.4 Jy km s^{-1} , corresponding to an HI mass of $3.3 \times 10^8 M_{\odot}$, assuming the companion lies at the distance of NGC 3640 listed in Table 1.

There is an unresolved radio continuum source that lies 47'' to the southeast of NGC 3640, outside its main body, but within the fainter optical isophotes, with a flux of 41 mJy at 1.4 GHz. There is no optical counterpart on the DSS image, and this is probably a background radio source.

4.3. *NGC 4382 = M85 = UGC 7508*

NGC 4382 is a member of the Virgo I group (LGG 292), with 126 cataloged members. Together with the elliptical VCC 797 (lying 2.9' to the south of NGC 4382) and

the barred spiral NGC 4394 (lying 7.6' to the east), it forms Redshift Survey Compact Group No. 54 (Barton et al. 1996). The dS0 galaxy IC 3292 is also likely associated (see Table 2). This makes this association a compact group within a subgroup of a moderately rich cluster. None of the other Virgo I group members fall within the primary beam (73 kpc radius at the adopted distance of 16.8 Mpc) and velocity coverage of the present HI observations.

Along with NGC 3640, NGC 4382 has the second highest value of the fine-structure index in the SS92 compilation ($\Sigma=6.85$, heuristic merger age 4–7 Gyr), with more than twelve irregular ripples, significant isophotal twists, and a plume to the north (Burstein 1979, Schweizer & Seitzer 1988), and exhibiting minor-axis rotation (Fisher 1997). It has centrally enhanced $H\beta$ and Mg_2 absorption, suggesting a relatively young ($< 3 \text{ Gyr}$) central population (Fisher, Franz & Illingworth 1996; Terlevich & Forbes 2002, hereafter TF02).

NGC 4382 has been observed numerous times with single dish telescopes, with the best limit obtained by Burstein, Krumm & Salpeter (1987), using Arecibo (3.3' HPBW) and sampling both the central position of NGC 4382 and pointings offset by 3' to each of the four compass points. No HI is detected associated with NGC 4382, resulting in limits of $\int S_{\text{HI}} dv < 0.2 \text{ Jy km s}^{-1}$ and $M_{\text{HI}}/L_B < 3 \times 10^{-4} M_{\odot} L_{\odot}^{-1}$. Burstein et al. claim a weak narrow HI feature in the pointing 3' south and close to the velocity of NGC 4382, which they tentatively associate with VCC 797.

We detect no HI emission associated with NGC 4382, to a limit of $\int S_{\text{HI}} dv < 0.12 \text{ Jy km s}^{-1}$, placing a limit of $M_{\text{HI}}/L_B < 2 \times 10^{-4} M_{\odot} L_{\odot}^{-1}$. We do not confirm the tentative detection of HI with VCC 797, nor do we detect the dS0 IC 3292. We do detect $4.8 \times 10^8 M_{\odot}$ of HI in the barred spiral NGC 4394 (also detected by Burstein et al. and others). The gas in this galaxy forms an asymmetric ring, with the HI concentrated to the spiral features outside of the bar (Fig. 3). The kinematics are very regular and symmetric, as seen in the intensity weighted velocity map (Figure 3) and the channel maps (Figure 4).

4.4. *NGC 5322 = UGC 8745*

NGC 5322 is the dominant elliptical of the NGC 5322 group (LGG 360), which has ten cataloged members. However, none of the other group members fall within the primary beam (140 kpc radius at the adopted distance of 31.6 Mpc) and velocity coverage of the present HI observations (but see below). NGC 5322 has a recently updated optical velocity from the Updated Zwicky Catalog (Falco et al. 1999) of 1781 km s^{-1} , whereas the HI observations were centered at the old RC3 value of 1915 km s^{-1} . This difference is still well within the observed band.

NGC 5322 has less obvious optical peculiarities than the other systems in this sample ($\Sigma=2.00$, heuristic merger age 5–8 Gyr). These include outer boxy and inner disk isophotes (Bender 1988). It also has peculiar stellar kinematics, with a small, counter-rotating disk embedded in a slowly rotating bulge (Bender 1988, Bender & Surma

1992, Rix & White 1992). There is a weak central radio source with symmetric jets aligned perpendicular to the central disk (Feretti et al. 1984), and the nuclear optical spectrum is characterized as a LINER. The central colors and [Mg/Fe] ratio of NGC 5322 suggest the presence of a 1–3 Gyr old central starburst population (Bender & Surma 1992, Silva & Bothun 1998a, 1998b). A luminosity weighted age of 4.2 ± 0.6 Gyr was estimated from fitting SSP models to 20 central line-strengths in NGC 5322 (Proctor & Sansom 2002), supporting the existence of a relatively young component.

NGC 5322 was previously searched for HI using the NRAO Greenbank 140 foot telescope (21' HPBW) by Knapp & Gunn (1982), obtaining an upper limit of $\int S_{\text{HI}} dv < 8.5 \text{ Jy km s}^{-1}$, resulting in the limit $M_{\text{HI}}/L_B < 0.022 M_{\odot} L_{\odot}^{-1}$.

We detect no HI emission associated with NGC 5322. The new HI limit is two orders of magnitude lower than the previous limit ($M_{\text{HI}}/L_B < 2 \times 10^{-4} M_{\odot} L_{\odot}^{-1}$). We do detect HI associated with two other nearby galaxies: MCG +10-20-039, an early type disk system lying 10.9' (100 kpc) to the south, and UGC 8714, a dwarf irregular lying 23.2' (210 kpc) to the northwest. MCG +10-20-039 has no previously determined redshift, while UGC 8714 is a known member of the NGC 5322 group. UGC 8714 was previously detected in the HI line by Schneider et al. (1992). See Fig. 1 for the integrated HI contoured on the DSS image, Figure 5 for channel maps of MCG +10-20-039, and Figure 6 for channel maps of UGC 8714. The HI kinematics of MCG +10-20-039 do not appear very organized, but this may be a result of our relatively coarse spatial resolution. The HI kinematics of UGC 8714 are characteristic of a highly inclined rotating disk.

4.5. NGC 7626 = UGC 12531

NGC 7626 is a one of the two brightest ellipticals in the Pegasus I cluster, lying just 6.9' (90 kpc at the adopted distance of 45.6 Mpc) and 420 km s⁻¹ away from the dominant elliptical galaxy of that cluster, NGC 7619. Both galaxies are part of the Pegasus group (LGG 473), with 25 cataloged members. However, the optical velocity of NGC 7619 ($V_{\odot}=3758 \text{ km s}^{-1}$) and most of the other cluster members fall outside of the high-velocity end of our bandpass ($V_{\odot} > 3730 \text{ km s}^{-1}$).

NGC 7626 has a modest amount of fine structure ($\Sigma=2.60$, heuristic merger age 7–9 Gyr). Its morphological peculiarities include outer and inner shells, a major-axis dust lane, and an inner 'X'-structure (Jedrzejewski & Schechter 1988; Forbes & Thomson 1992; Balcells & Carter 1993; Forbes, Franx & Illingworth 1995). HST imaging reveals a symmetric dust feature within the inner 0.5'' (Forbes et al. 1995, Carollo et al. 1997). This galaxy is noted for its very strange velocity field, which exhibits core rotation about an intermediate axis, and has shell-like regions of distinct kinematics around the core (Jedrzejewski & Schechter 1988, Balcells & Carter 1993, Longhetti et al 1998). The kinematically decoupled core has an enhanced Mg₂ index relative to the outer regions

(Davies Sadler & Peletier 1993), suggesting that its formation was accompanied by rapid star formation. Single stellar population models of the core, inner, and global line indices suggest uniformly old ages for the central stellar populations of both NGC 7626 and NGC 7619 (7–12 Gyr; Gonzalez 1993, Longhetti et al. 2000, Trager et al. 2000, TF02).

NGC 7626 is a radio galaxy, with two symmetric jets on either side of a central core (Jenkins 1982, Birkinshaw & Davies 1985). Our radio continuum map is shown contoured on the DSS image in Figure 7. The lobes are edge brightened and extend 8.0' (106 kpc) to the northeast and 6.3' (84 kpc) to the southwest. The core has a flux of 290 mJy at the observed sky frequency of 1404 MHz, while the entire radio structure has a total flux of 1.12 Jy. The radio jet is tilted by $\sim 35^{\circ}$ with respect to the dust lane imaged by HST (Forbes et al. 1995, Carollo et al. 1997). NGC 7619 has an unresolved radio continuum source with a flux of 25 mJy. NGC 7626 has a compact X-ray source at its center, most likely associated with the central engine, while NGC 7619 is a strong, extended X-ray source with an X-ray 'tail' (Trinchieri et al. 1997).

The region around and between NGC 7626 and NGC 7619 was mapped in the HI line by Kumar & Thonnard (1983) with Arecibo (3.3' HPBW). No HI was detected at any of the eleven pointings, with resulting limit of $\int S_{\text{HI}} dv < 1.1 \text{ Jy km s}^{-1}$. A more stringent limit was set with the Effelsberg 100-m telescope (9.3' HPBW) by Huchtmeier (1995) using a single pointing on NGC 7626, giving $\int S_{\text{HI}} dv < 0.7 \text{ Jy km s}^{-1}$ and $M_{\text{HI}}/L_B < 0.007 M_{\odot} L_{\odot}^{-1}$.

We report a tentative detection of faint HI emission outside optical body of NGC 7626. Figure 1 presents the integrated HI emission contoured upon the DSS image, including both NGC 7626 (east) and NGC 7619 (west). Figure 7 shows a greyscale image of the DSS with the integrated HI emission as thick contours along with thinner contours for the radio continuum emission. Figure 8 shows the channel maps over a field containing both NGC 7626 and NGC 7619. Since the single beam, single channel flux is weak (with a peak line flux of 2 mJy beam⁻¹ or 4.3 sigma), the channel maps do not convincingly show the HI emission. We therefore present two other figures: Figure 9 showing a position-velocity profile through the peak emission and parallel to the right ascension axis, and Figure 10 showing a spectra extracted over the region containing the two features in the moment map. The optical velocity of NGC 7626 is indicated in both plots (by a dashed line in Fig. 9 and by an arrow in Fig. 10). While the emission is of low signal-to-noise, it appears in several adjacent channels. Still, the detection is considered tentative and should be confirmed by additional observations.

The neutral hydrogen emission lies between NGC 7626 and NGC 7619 in both space and velocity: the emission peak is at 23:20:32.6 +08:12:00 (J2000) and $V_{\odot}=3518 \text{ km s}^{-1}$. This is 2.7' (36 kpc) and +85 km s⁻¹ from the optical center of NGC 7626 (Table 2), and 4.4' (59 kpc) and -240 km s⁻¹ from NGC 7619. The flux integrated over the spec-

tra of Fig. 10 is $0.17 \text{ Jy km s}^{-1}$, which is consistent with the single dish upper limits mentioned above. This flux corresponds to an HI mass of $8.3 \times 10^7 M_{\odot}$ at the distance of NGC 7626. Curiously, the HI cloud lies just to the side of the radio jet (Fig. 7). A very similar situation occurs in the shell Galaxy Cen A (NGC 5128; Schiminovich et al. 1994).

We detect HI in one other cluster member, the Sb galaxy NGC 7631 lying $11'$ (145 kpc) to east. This emission appears at the edge of our bandpass, so we do not map the full extent of HI line emission, and as such the HI flux and mass reported in Table 2 are lower limits. Channel maps for this galaxy are presented in Figure 11. The HI kinematics are characteristic of half of a rotating disk, with the higher velocity half falling outside of our observing band. Three other cluster members fall within the primary beam and velocity coverage of our HI observations, but are not detected (see Table 2).

5. DISCUSSION

5.1. HI in the NGC 7626 System

The detection of HI outside the optical body of NGC 7626 was something of a surprise. However, our earlier study on the global properties of the SS92 sample turned up a few shell systems with HI located outside their optical bodies (Table 2 of Sansom et al. 2000). Maps of these systems and other interesting examples appear in the ‘‘HI Rogues Gallery’’ (Hibbard et al. 2001a), in the category ‘‘Peculiar Early Types with HI Outside their Optical Body’’ (Nos. 112–120 in the Rogues Gallery). This category is arranged in a sequence ranging from systems with abundant quantities of HI in the outer regions to systems with little or no HI in the outer regions, with NGC 7626 appearing near the end of the sequence.

There are a number of systems in this sequence which are quite similar to NGC 7626. Some specific examples are NGC 470/4, NGC 1316, NGC 4125, and M 86. NGC 474 is a spectacular shell system in the sample of SS92, with $\Sigma = 5.26$ and a heuristic merger age of 4–5 Gyr. There are HI clouds that appear to have been torn off the nearby Sb galaxy NGC 470 and distributed at several locations around the galaxy, but the HI does not appear to make it into the optical body of the galaxy (Schiminovich et al. 2001). Similarly, NGC 1316 (Fornax A) is a well known peculiar system with many shells, ripples and plumes with good evidence that it is a $\lesssim 3$ Gyr merger remnant (Schweizer 1980, Goudfrooij et al. 2000a,b). There are HI clumps around it that may have been torn from the nearby S0/a galaxy NGC 1317, but again these clouds avoid the main optical body of NGC 1316 (Horellou et al. 2001). NGC 4125 is a shell galaxy in the sample of SS92, with $\Sigma = 6.00$ and a heuristic merger age of 6–8 Gyr. Unlike the other systems, it is apparently isolated. It has a few small HI clouds outside its optical body (Rupen, Hibbard & Bunker 2001). M 86 (a.k.a. NGC 4406) is a large early type galaxy in the Virgo cluster. It has an X-ray ‘‘tail’’ to the northwest and an HI cloud to the

south, outside the main body of M 86 (Li & van Gorkom 2001). NGC 7626 may also bear some resemblance to the radio galaxy Coma A, where HI has been detected in absorption against the radio lobes, some ~ 30 kpc from the galaxy center (Morganti et al. 2002).

While there are systems similar to NGC 7626, the nature of the intergalactic HI clouds is not at all clear. They could be diffuse remnant tidal debris which only remains neutral far outside of the body of the elliptical, becoming photoionized by the stellar population at smaller radii (Hibbard, Vacca & Yun 2000); or they could be a result of complex multiphase hydrodynamics, such as a jet-ISM, jet-ICM, or galaxy-ICM interaction. In this respect, X-ray imaging of the Pegasus group would be very instructive.

5.2. HI in fine-structure ellipticals

We expected a fair detection rate in these high Σ ellipticals. This presumption was based primarily on two considerations: (1) peculiar E/SO galaxies have a 45% HI detection rate (Bregman, Hogg, & Roberts 1992; van Gorkom & Schiminovich 1997), and (2) the expectation that the highest Σ systems would be the youngest remnants of disk mergers, and therefore most likely to still have gas-rich tidal debris. Therefore, we were somewhat surprised that only one of the five fine-structure galaxies that we targeted was detected in HI. Moreover, the detected system, NGC 7626, is on the low end of the Σ scale, and we failed to detect HI in the three highest Σ systems in the compilation of SS92 (NGC 3610, NGC 3640 and NGC 4384).

While the number of systems that we observed in the present program is much too small to draw any statistical conclusions, in our previous study (Sansom, Hibbard & Schweizer 2000) we examined all of the available HI mapping data for galaxies in the lists of SS92. We found that 17/37 (46% \pm 16%) were detected in HI (i.e., the same fraction as found by Bregman et al. for peculiar E/SOs). The HI morphology suggests a tidal origin in all but three of these detections. However, the SS92 compilation includes early types with a wide range of Σ . When plotting cold and hot gas properties versus Σ , we find no correlation besides the previously known tendency for recent ($\lesssim 3$ Gyr) merger remnants to be X-ray faint (Fabbiano & Schweizer 1995; Georgakakis, Forbes & Norris 2000; O’Sullivan, Forbes & Ponman 2001, see also <http://www.star.uclan.ac.uk/~aes/GALS/ISM.html>).

One possibility is that tidal HI does not survive for as long in the outer regions as inferred from studies of young, more isolated merger remnants (Hibbard & Mihos 1995). Another possibility is that a high fine structure index does not unambiguously identify recent disk-disk merger remnants. We look at each of these possibilities in turn.

Regarding the longevity of tidal material, in their dynamic study of the merger remnant NGC 7252, Hibbard & Mihos (1995) found that the outermost HI-rich material should remain at large radii from the remnant, evolving on timescales of several Gyr. However, that study only considered the effects of gravity, and did not address the

survivability of the gas in its neutral form. As the tidal debris evolves, it becomes more diffuse. At low HI column densities, this gas may be susceptible to ionization by the intergalactic UV field (Hill 1974, Bland-Hawthorn & Maloney 1999), or even by the stellar population of the remnant (Hibbard, Vacca & Yun 2000). Perhaps more importantly, NGC 7252 is a relatively isolated system, while the five systems studied here are in groups or clusters. In such environments, the crossing times are of the same order as the timescale for tidal evolution, and it may be difficult for tidal HI to maintain a coherent morphology for very long (see also Verdes-Montenegro et al. 2001). We believe these effects contribute to the lack of detectable tidal HI in the targeted galaxies. In this case, such gas should give rise to extensive ionized haloes around galaxies (Morris & van den Bergh 1994, Tadhunter et al. 2000), which may be detectable in absorption against background sources (e.g. Norman et al. 1996, Carilli & van Gorkom 1993). If we could accurately date the time since the merger, it would help evaluate the likelihood of this possibility.

Regarding the ability of a high fine-structure index to pick out the youngest merger remnant, we re-evaluate the relationship between fine-structure index and population age indicators² derived by SS92. The heuristic merger ages tabulated by SS92 were based on broad band *UBV* colors, which are not straight forward to interpret in terms of ages, because of age-metallicity degeneracies, non-solar abundances and ratios, line emission, dust, frosting of a young population, etc. (see Worthey 1994 and Proctor & Sansom 2002 for discussions of some of these effects). Spectroscopic ages are now available using several line indices sensitive to both age and metallicity. We therefore re-evaluate the relationship between fine-structure index and population age using these new age indicators.

For our age indicators, we use the sample of early type galaxies with uniform quality line-strength data assembled from the literature by TF02, for which luminosity weighted ages have been determined using the SSP models of Worthey (1994)³. We emphasize that these are not absolute ages, but age indicators: derived ages will differ for different models, but the relative age ranking should be maintained (see TF02 for a discussion of these points). We therefore do not augment this sample by including galaxies with merger ages estimated by a different method. Figure 12 shows how the fine-structure index compares with the logarithm of the spectroscopically determined ages ($\log[\text{Age}_{SP}]$) for the 26 galaxies in the TF02 sample which also have fine-structure quantified by SS92.

A statistical test on Σ and Age_{SP} for these 26 systems shows that they are highly anti-correlated (Spearman rank-order correlation coefficient $r_s = -0.70$). However, the correlation drops when the young merger remnants NGC 3921 and NGC 7252 are dropped from the sample ($r_s =$

0.62). Unlike the other systems in the SS92 sample, these two systems were included based on their status as known merger remnants. Further analysis indicates that most of the anti-correlation between Σ and Age_{SP} comes from systems with high Σ ($\gtrsim 4$) and young ages ($\lesssim 3$ Gyr; $r_s = -0.83$); the rank order correlation coefficient drops to $r_s = -0.14$ for systems with lower Σ and higher Age_{SP} . Therefore, the apparent anti-correlation may be due to the purposeful inclusion of the well-known merger remnants NGC 7252 and NGC 3921 by both SS92 and TF02 at the high- Σ , low spectroscopic age end, and to the very few systems with a fine-structure index in the range $6 \lesssim \Sigma \lesssim 8$. Indeed, three of our systems fall within the range: NGC 3610, NGC 3640, NGC 4382 (Table 1). NGC 4382 is one of the points in the plot, while NGC 3610 and NGC 3640 would lie well above the apparent relationship if the age indicators given in §4 are taken (i.e., 4–7 Gyr for NGC 3610, and 6–8 Gyr for NGC 3640). So while Fig. 12 reinforces the use of fine structure for tracking dynamically young remnants, it would be more reassuring to have more objects with a high fine-structure, and to have better age indicators than luminosity weighted mean ages.

In conclusion, we cannot say unambiguously that the five fine-structure ellipticals studied here are “King Gap” objects (i.e., evolved remnants of major disk-disk mergers). They may indeed be the result of gas-rich mergers, but evolved enough that any tidal gas that was thrown out during the encounter has fallen back, dispersed, or been converted to other forms. However, they may have had quite different histories, including minor mergers or major mergers of gas-poor progenitors. Together, these results suggest that progenitor type, encounter geometry, and local environment may all play an important role in the expected post-merger evolution, and that there is not one simple path from disk mergers to old ellipticals (see also Hibbard et al. 2001a; Verdes-Montenegro et al. 2001). These possibilities can only be constrained by investigating young objects in the so-called “King Gap”. To this end, Fig. 12 offers some hope. Clearly, interacting systems may evolve in many ways in this plane, depending on what merged and how many stars, if any, were made during the interaction. Less drastic interacting histories may leave remnants anywhere along the right hand side of this plot, making it harder to determine the origin of such systems. However, major mergers of gas-rich systems *must* evolve from the lower left of the plot to the upper right.

It is not clear *how* remnants will evolve in this plane, or whether Σ and spectroscopically determined SSP ages are the best parameters to evaluate: Σ may not properly capture the dynamical evolution of the optical peculiarities and, given the range of possible progenitors and encounter geometries, perhaps no single parameter can; additionally,

²Here we make the usual assumption that disk-disk mergers must be accompanied by a significant burst of star formation, lowering the luminosity weighted mean age of the central stellar population. This is a gross simplification, since merger-induced star formation histories are likely quite complex. The derived “ages” should be considered as age indicators, rather than actual ages.

³We note that the TF02 line indices have been converted to measurements within the inner $R_e/8$ of the systems, where R_e is the effective radius of the galaxy, and therefore are most sensitive to the ages of the central stellar population.

mergers of gas rich systems may have complicated star formation histories (e.g. Mihos & Hernquist 1996) that are poorly constrained by simple stellar population models (see also Liu & Green 1996), and luminosity weighted mean population ages may only be roughly related to the time since the latest merger event (Hibbard et al. 2001b). But the above considerations reinforce the suggestion of SS92 that signs of both dynamical youth and a youthful population should be used to identify the youngest “King Gap” objects.

6. SUMMARY

We detected neutral hydrogen in the vicinity of four of the five fine-structure E/SO galaxies which we observed with the VLA D-array. In only one case is the HI directly associated with the targeted elliptical. For this one case, NGC 7626, there is a tentative detection of HI outside the optical body of the galaxy. This system contains a kinematically distinct core, but no obvious signs of being a recent merger, and its stellar population is uniformly old (at least as indicated by SSP determined ages). Therefore the origin of the HI is unclear, but similar systems are known from the literature.

Combining the present results with the analysis of Sansom, Hibbard & Schweizer 2000, we find that galaxies with a large value of the fine-structure parameter, Σ , are no more likely to be detected in HI than those with a low value of Σ . This suggests that if the high Σ ellipticals are aged remnants of disk-disk mergers, their tidal HI did not survive longer than a few Gyrs. This may be due to the short crossing time in the group environment, and/or due to ionization of the HI as it becomes more diffuse. This gas would contribute to a very diffuse neutral or ionized halo around the remnants.

Given these results, we conclude that the most promising way to constrain the observational characteristics of aged remnants of *gas-rich* mergers would be to target younger “King Gap” objects (ages $\lesssim 2$ Gyr) which contain signatures of both a dynamical youth and a youthful central stellar population. A growing population of ob-

jects is being identified, both by the appearance of optical and gaseous tidal features (e.g. Schiminovich et al. 2001, Chang et al. 2001, Hibbard et al. 2001a), and by spectroscopic studies of peculiar or normal early type galaxies (e.g. Bergval, Ronnback & Johansson 1989; Oegerle, Hill & Hoessel 1991; Zabludoff et al. 1996; Longhetti et al. 1998, 2000; Hau et al. 1999; Trager et al. 2000; Georgakakis et al. 2001; TF02; Proctor & Sansom 2002).

Once a population of recent merger remnants is identified, they would enable us to judge the appearance of merger remnants at ages of $\gtrsim 2$ Gyr. By examining the cold gas content and distribution, global colors and line indices, inner/outer color differences, and light profiles of such systems, we could evaluate whether they are likely to evolve into normal ellipticals, or if instead they will leave long-lived signatures of their merger origin (Mihos & Hernquist 1994, Hibbard & Yun 1999, van den Marel & Zurek 2000, Mihos 2001). By identifying the expected observational signatures along the post-merger path we may ultimately be able to determine the fraction of the elliptical galaxy population which had a merger origin.

Our thanks to the staff at the VLA for their help in obtaining these observations and for help during our preliminary analysis. We thank F. Schweizer, J. van Gorkom and D. Schiminovich for many fruitful conversations and for comments on earlier drafts of this paper.

The VLA of the National Radio Astronomy Observatory is operated by Associated Universities, Inc., under cooperative agreement with the National Science Foundation. This research has made use of the NASA/IPAC Extragalactic Database (NED), which is operated by the Jet Propulsion Laboratory, California Institute of Technology, under contract with the National Aeronautics and Space Administration. Optical images were taken from the Digitized Sky Surveys, produced at the Space Telescope Science Institute under U.S. Government grant NAG W-2166. The images of these surveys are based on photographic data obtained using the Oschin Schmidt Telescope on Palomar Mountain.

REFERENCES

- Balcells, M., & Carter, D. 1993, *A&A*, 279, 376
 Balcells, M., van Gorkom, J.H., Sancisi, R., & del Burgo, C., 2001, *AJ*, 122, 1758
 Barnes J. E., Hernquist L., 1991, *ApJ*, 370, L65
 Barton, E., Geller, M. J., Ramella, M., Marzke, R. O., & Da Costa, L. N. 1996, *AJ*, 112, 871
 Bender, R. 1988, *A&A*, 202, L5
 Bender R., & Surma P., 1992, *A&A*, 258, 250
 Bergvall, N., Ronnback, J., & Johansson, L. 1989, *A&A*, 222, 49
 Binggeli, Sandage, Tammann, 1985, *AJ*, 90, 1681
 Biegging, J. H. 1978, *A&A*, 64, 23
 Birkinshaw, M., & Davies, R. L. 1985, *ApJ*, 291, 32
 Bland-Hawthorn, J., & Maloney, P.R. 1999, *ApJ*, 510, 33
 Bregman, J. N., Hogg, D. E., & Roberts, M. S. 1992, *ApJ*, 387, 484
 Briggs, D. 1995, PhD Thesis, New Mexico Tech
 Brown B. A., & Bregman J. N., 1998, *ApJ*, 495, L75
 Burstein, D. 1979, *ApJS*, 41, 435
 Burstein, D., Krumm, N., & Salpeter, E. E. 1987, *AJ*, 94, 883
 Carilli, C. L., & van Gorkom, J. H. 1992, *ApJ*, 399, 373
 Carollo, C. M., Danziger, I. J., Rich, R. M., & Chen, X. 1997, *ApJ*, 491, 545
 Chang, T.-C., van Gorkom, J. H., Zabludoff, A. I., Zaritsky, D., & Mihos, J. C. 2001, *AJ*, 121, 1965
 Davies, R. L., Sadler, E. M., & Peletier, R. F. 1993, *MNRAS*, 262, 650
 de Vaucouleurs, G., de Vaucouleurs, A., & Corwin Jr, H. G., Buta, R. J. Paturel, G., & Fouque, P. 1991, *Third Reference Catalogue of Bright Galaxies* (New York: Springer Verlag) (RC3)
 Dupraz, C., & Combes, F. 1986, *A&A*, 166, 53
 Fabbiano G., & Schweizer F., 1995, *ApJ*, 447, 572
 Falco, E.E. et al. 1999, *PASP*, 111, 438. The Updated Zwicky Catalog
 Feretti, L., Giovannini, G., Hummel, E., & Kotanyi, C. G. 1984, *A&A*, 137, 362
 Fisher, D. 1997, *AJ*, 113, 950
 Fisher, D., Franx, M. & Illingworth, G. 1996, *ApJ*, 459, 110
 Forbes, D., Franx, M. & Illingworth, G. 1995, *AJ*, 109, 1988
 Forbes, D. A., & Thomson, R. C. 1992, *MNRAS*, 254, 723
 Garcia, A. M. 1993, *A&AS*, 100, 47 (LGG)
 Geller, M. J., & Huchra, J. P. 1983, *ApJS*, 52, 61
 Gonzalez, J. J., 1993, Ph.D. Thesis, Univ. California, Santa Cruz
 Goudfrooij, P., Alonso, M. V., Maraston, C., & Minniti, D. 2001a, *MNRAS*, 328, 237

- Goudfrooij, P., Mack, J., Kissler-Patig, M., Meylan, G., & Minniti, D. 2001b, *MNRAS*, 322, 643
- Georgakakis, A., Forbes, D.A., & Norris, R.P. 2000, *MNRAS*, 318, 124
- Georgakakis, A., Hopkins, A. M., Caulton, A., Wiklind, T., Terlevich, A. I., & Forbes 2001, *MNRAS*, 326, 1431
- Hau G.K.T., Carter D., Balcells M., 1999, *MNRAS*, 306, 437
- Hernquist, L., & Quinn, P. J. 1988, *ApJ*, 331, 682
- Hernquist, L., & Quinn, P. J. 1989, *ApJ*, 342, 1
- Hernquist, L., & Spergel, D. N. 1992, *ApJ*, 399, L117
- Hibbard J. E., & Mihos J. C., 1995, *AJ*, 110, 140
- Hibbard, J. E. & van Gorkom, J. H. 1996, *AJ*, 111, 655
- Hibbard, J.E., van Gorkom, J.H., Rupen, M.P. & Schiminovich, D. 2001a, in *ASP Conf. Ser. Vol. 240, Gas & Galaxy Evolution*, ed. J.E. Hibbard, M.P. Rupen, & J.H. van Gorkom, (ASP, San Francisco), 659
- Hibbard, J. E., Guhathakurta, P., van Gorkom, J. H., & Schweizer, F. 1994, *AJ*, 107, 67
- Hibbard, J. E., Vacca, W. D., & Yun, M. S. 2000, *AJ*, 119, 1130
- Hibbard, J. E., van der Hulst, J. M., Barnes, J. E., & Rich, R.M. 2001b, *AJ*, 122, 2969
- Hibbard, J. E., & Yun, M. S. 1999, *ApJ*, 522, L93
- Hill, J. K. 1974, *A&A*, 34, 431
- Horellou, C., Black, J. H., van Gorkom, J. H., Combes, F., van der Hulst, J. M., & Charmandaris, V. 2001, *A&A*, 376, 837
- Huchtmeier, W. K. 1995, *A&A*, 286, 389
- Huchtmeier, W. K., & Richter, O. -G. 1989, "A General Catalog of HI Observations of Galaxies" (New York: Springer-Verlag)
- Jedrzejewski, R. & Schechter, P. L. 1988, *ApJ*, 330, L87
- Jenkins, C. R., 1982, *MNRAS*, 200, 705
- Knapp, G. R., & Gunn, J. E. 1982, *AJ*, 87, 1634
- Kumar, C. K., & Thonnard, N., 1983, *AJ*, 88, 260
- Lake, G., & Schommer, R. A., 1984, *ApJ*, 280, 107
- Li, Y., & van Gorkom, J. H. 2001, in *ASP Conf. Ser. Vol. 240, Gas & Galaxy Evolution*, ed. J.E. Hibbard, M.P. Rupen, & J.H. van Gorkom, (ASP, San Francisco), 637
- Lim, J., & Ho, P. T. P. 1999, *ApJ*, 510, L7
- Liu, C. T., & Green, R. F. 1996, *ApJ*, 458, L63
- Longhetti, M., Rampazzo, R., Bressan, A., & Chiosi, C., 2000, *A&A*, 353, 917
- Longhetti, M., Rampazzo, R., Bressan, A., & Chiosi, C., 1998, *A&AS*, 130, 267
- Malin, D. F. 1978, *Nature*, 276, 591
- Malin, D. F. 1979, *Nature*, 277, 279.
- Malin, D. F., & Carter, D. 1980, *Nature*, 285, 643
- Malin, D. F., & Carter, D. 1983, *ApJ*, 274, 534
- Martin, M. C., 1998, *A&AS*, 131, 73
- Mihos, J. C. 2001, in *ASP Conf. Ser. Vol. 240, Gas & Galaxy Evolution*, ed. J.E. Hibbard, M.P. Rupen, & J.H. van Gorkom, (ASP, San Francisco), 143
- Mihos J. C. & Hernquist L., 1996, *ApJ*, 464, 641
- Mihos, J. C., Hernquist, L. 1994, *ApJ*, 437, L47
- Miller, B. W., Whitmore, B. C., Schweizer, F., & Fall, S. M. 1997, *AJ*, 114, 2381
- Morganti, R., Oosterloo, T.A., Tinti, S., Tadhunter, C.N., Wills, K.A., & van Moorsel, G. 2002, *A&A*, 387, 830
- Morris, S. L., & van den Bergh, S. 1994, *ApJ*, 427, 696
- Norman, C., Bowen, D. V., Heckman, T., Blades, C., & Danly, L. 1996, *ApJ*, 472, 73
- O'Sullivan, E., Forbes, D. A., & Ponman, T. J. 2001, *MNRAS*, 324, 420
- Oegerle, W. R., Hill, J. M., & Hoessel, J. G. 1991, *ApJ*, 381, L9
- Proctor, R.N., & Sansom A.E. 2002, *MNRAS*, 333, 517
- Prugniel, P., Nieto, J.-L., Bender, R., & Davoust, E. 1988, *A&A*, 204, 61
- Quinn, P. J. 1984, *ApJ*, 279, 596
- Read, A. M., & Ponman, T. J. 1998, *MNRAS*, 297, 143
- Reid, N., Boisson, C. & Sansom, A. E. 1994, *MNRAS*, 269, 713
- Rix, H.-W., & White, S. D. M., 1992, *MNRAS*, 254, 389
- Roberts, M. S., Hogg, D. E., Bregman, J. N., Forman, W. R., & Jones, C. 1991, *ApJS*, 75, 751
- Rupen, M. P. 1999, in *Synthesis Imaging in Radio Astronomy*, ASP Conf. Series vol. 180, ed. G. B. Taylor, C. L. Carilli and R. A. Perley (ASP, San Francisco), 229
- Rupen, M. P., Hibbard, J. E., & Bunker, K. 2001, in *ASP Conf. Ser. Vol. 240, Gas & Galaxy Evolution*, ed. J.E. Hibbard, M.P. Rupen, & J.H. van Gorkom, (ASP, San Francisco), 864
- Sansom, A. E., Hibbard, J. E., & Schweizer, F. 2000, *AJ*, 120,
- Schiminovich, D. 2001, in *ASP Conf. Ser. Vol. 240, Gas & Galaxy Evolution*, ed. J.E. Hibbard, M.P. Rupen, & J.H. van Gorkom, (ASP, San Francisco), 147
- Schiminovich D., van Gorkom J.H., van der Hulst J.M., Kasaw S., 1994, *ApJ*, 423, L101
- Schiminovich D, van Gorkom J.H., van der Hulst J.M., Malin D.F., 1995, *ApJ*, 444, L77
- Schiminovich, D., van Gorkom, J. H., Dijkstra, M., Li, Y., Petric, A., & van der Hulst, J. M. 2001, in *ASP Conf. Ser. Vol. 240, Gas & Galaxy Evolution*, ed. J.E. Hibbard, M.P. Rupen, & J.H. van Gorkom, (ASP, San Francisco), 864
- Schneider, S. E., Thuan, T. X., Mangum, J. G., & Miller, J. 1992, *ApJS*, 81, 5
- Schweizer, F. 1982, *ApJ*, 252, 455
- Schweizer, F. 1996, *AJ*, 111, 109
- Schweizer, F. 1998, in *Saas-Fee Advanced Course No. 26, Galaxies: Interactions and Induced Star Formation*, R. C. Kennicutt Jr., F. Schweizer and J. E. Barnes (Springer, Berlin), 105
- Schweizer, F. 1980, *ApJ*, 237, 303
- Schweizer, F., & Ford, W. K., Jr. 1984, *Lecture Notes in Physics No. 232, New Aspects of Galaxy Photometry*, ed. J. -L. Nieto (Springer, Berlin), 145
- Schweizer, F., Miller, B. W., Whitmore, B. C., & Fall, S. M. 1996, *AJ*, 112, 1839
- Schweizer, F., & Seitzer, P. 1988, *ApJ*, 328, 88
- Schweizer F., Seitzer P., 1992, *AJ*, 104, 1039 (SS92)
- Schweizer, F., Seitzer, P., Faber, S. M., Burstein, D., Dalle Ore, C. M., & Gonzalez, J. J. 1990, *ApJ*, 364, L33
- Scorza, C., & Bender, R. 1990, *A&A*, 235, 49
- Shostak, G. S., Roberts, M. S., & Peterson, S. D. 1975, *AJ*, 80, 581
- Silva, D. R., & Bothun, G. D. 1998a, *AJ*, 116, 85
- Silva, D. R., & Bothun, G. D. 1998b, *AJ*, 116, 2793
- Smith, R. J., Lucey, J. R., Hudson, M. J., Schlegel, D. J., & Davies, R. L. 2000, *MNRAS*, 313, 469
- Tadhunter, C.N., Villar-Martin, M., Marganti, R., Bland-Hawthorn, J. & Axon, D. 2000, *MNRAS*, 314, 849
- Taylor, G. B., Carilli, C. L. & Perley, R. A., 1999, eds, *ASP Conf. Series vol. 180, Synthesis Imaging in Radio Astronomy*, (ASP, San Francisco)
- Terlevich, A. I., & Forbes, D. A. 2002, *MNRAS*, 330, 547 and <http://astronomy.swin.edu.au/staff/dforbes/agecat.html> (TF02)
- Toomre, A. 1977, in *The Evolution of Galaxies and Stellar Populations*, ed. B. M. Tinsley & R. B. Larson (Yale University Press, New Haven), 401
- Toomre, A., & Toomre, J. 1972, *ApJ*, 178, 623
- Trager, S. C., Faber, S. M., Worthey, G., & Gonzalez, J. J. 2000, *AJ*, 119, 1645
- Trinchieri, G., Fabbiano, G., & Kim, D-W. 1997, *A&A*, 318, 361
- Tully, R. B. 1988, *Nearby Galaxies Catalog* (Cambridge: Cambridge Univ. Press)
- van den Marel, R. P., & Zurek, D. 2000, in *ASP Conf. Ser. 197, Dynamics of Galaxies: from the Early Universe to the Present*, eds. F. Combes, G. A. Mamon, & V. Charmandaris (SF: ASP), 323
- van Gorkom, J., & Schiminovich, D., 1997, in *ASP Conf. No. 116, The Nature of Elliptical Galaxies*, eds. M. Arnaboldi, G. S. Da Costa and P. Saha, 310
- Verdes-Montenegro, L., Yun, M. S., Williams, B. A., Huchtmeier, W. K., Del Olmo, A., & Perea, J. 2001, *A&A*, 377, 812
- Whitmore, B. C., Miller, B. W., Schweizer, F., Fall, S. M. 1997, *AJ*, 114, 1797
- Whitmore B.C., Schweizer F., Kundu A., Miller B.W. 2002, *AJ*, 124, 147
- Worthey, G. 1994, *ApJS*, 95, 107
- Yun, M. S., Hibbard, J. E. 2001, *ApJ*, 550, 104
- Zabludoff, A. I., Zaritsky, D., Lin, H., Tucker, D., Hashimoto, Y., Shectman, S. A., Oemler, A. A., & Kirshner, R. P. 1996, *ApJ*, 466, 104

TABLE 1
SAMPLE PROPERTIES

Parameter	NGC 3610	NGC 3640	NGC 4382	NGC 5322	NGC 7626
Hubble Type (RC3)	E5:	E3	SA(s)0+pec	E3-4	E1 pec
Optical Velocity ^a (km s ⁻¹)	1696	1314	729	1781	3433
Distance ^b (Mpc)	29.2	24.2	16.8	31.6	45.6
Fine-structure index ^c (Σ)	7.6	6.85	6.85	2.00	2.60
Environment ^d	LGG 234 (N3642 group)	LGG 233 (N3640 group)	LGG 292 (Virgo I group)	LGG 360 (N5322 group)	LGG 473 (Pegasus group)
Known group members ^d	N=5	N=7	N=126	N=10	N=25
Observed Date	1997 Dec 3	1997 Dec 3	1997 Dec 3	1997 Dec 3	1997 Dec 7
Velocity Center ^e (km s ⁻¹)	1787	1314	760	1915	3423
Velocity Coverage ^f (km s ⁻¹)	1516-2090	1044-1616	491-1061	1644-2218	3159-3729
Phase Center:					
RA (J2000)	11 18 25.9	11 21 06.8	12 25 24.7	13 49 15.6	23 20 42.4
DEC (J2000)	+58 47 14	+03 14 08	+18 11 27	+60 11 29	+08 13 02
Time on Source	2h 32m	2h 22m	1h 57m	2h 22m	2h 11m
Flux Calibrator	1331+305	1331+305	1331+305	1331+305	0137+331
Phase Calibrator	1206+642	1120+143	1254+116	1411+522	2253+161
Bandpass Calibrator	1206+642	1120+143	1331+305	1411+522	2253+161
Bandwidth (MHz)	3.25	3.25	3.25	3.25	3.25
Number of Channels	63	63	63	63	63
Channel Spacing (km s ⁻¹)	10.4	10.4	10.4	10.4	10.5
Synthesized Beam					
(major \times minor axis)	66'' \times 49''	62'' \times 49''	54'' \times 50''	57'' \times 50''	55'' \times 49''
rms noise (mJy beam ⁻¹)	0.60	0.63	0.65	0.58	0.46

^aOptical velocities for NGC 3610 and NGC 5322 are from the Updated Zwicky Catalog (Falco et al. 1999), for NGC 4382 and NGC 7626 are from Smith et al. (2000), and from the RC3 for NGC 3640.

^bDistances taken from the *Nearby Galaxy Catalog* (Tully 1988), except for NGC 7626, where the optical velocity from the RC3 is used, assuming a Hubble constant of $H_o = 75 \text{ km s}^{-1} \text{ Mpc}^{-1}$.

^cFine-structure index from Table 1 of SS92.

^dEnvironment taken from Loose Galaxy Group catalog (Garcia, 1993), number of known group members taken from NED.

^eThe central velocity for the HI observations were based on the best available optical velocities at the time of the observations, which were from the RC3 for all galaxies except NGC 4382, which was taken from Binggeli, Sandage and Tammann (1985).

^fVelocity coverage from channels 3-55 of HI datacube.

TABLE 2
VLA HI OBSERVATIONS^a

(1) Galaxy	(2) Hubble Type	(3) Field	(4) V_{opt} (km s ⁻¹)	(5) V_{HI} (km s ⁻¹)	(6) ΔW (km s ⁻¹)	(7) dr (arcmin)	(8) ρ (kpc)	(9) $(S_{HI}\Delta v)$ (Jy km s ⁻¹)	(10) M_{HI} (M_{\odot})
NGC 3610	E5:	NGC 3610	1696	—	—	0	0	<0.04	< 2 × 10 ⁷
NGC 3640	E3	NGC 3640	1314	—	—	0	0	<0.05	< 1 × 10 ⁷
N3640 comp ^b	uncataloged	NGC 3640	—	1180	62	15.1	105	2.4	3.3 × 10 ⁸
NGC 4382	S0+pec	NGC 4382	729	—	—	0	0	<0.06	< 1 × 10 ⁷
VCC 0797	E?	NGC 4382	773	—	—	2.9	14	<0.06	< 1 × 10 ⁷
NGC 4394	SBb	NGC 4382	922	915	165	7.6	37	7.2	4.8 × 10 ⁸
IC 3292	dS0	NGC 4382	710	—	—	8.5	42	<0.07	< 1 × 10 ⁷
NGC 5322	E3-4	NGC 5322	1781	—	—	0	0	<0.04	< 2 × 10 ⁷
MCG+10-20-039	unclassified	NGC 5322	—	1870	100	10.9	100	0.43	1.0 × 10 ⁸
UGC 8714	Im	NGC 5322	2044	2030	210	23.2	215	4.7	1.1 × 10 ⁹
NGC 7626	E1 pec	NGC 7626	3433	3518	105	2.7	36	0.17	8.3 × 10 ⁷
AGC 330257	unclassified	NGC 7626	3470	—	—	3.9	52	<0.04	< 3 × 10 ⁷
NGC 7631 ^c	Sb	NGC 7626	3754	>3700	>200	11.0	145	>1.9	> 9.3 × 10 ⁸
NGC 7623	S0 ⁰ :	NGC 7626	3739	—	—	11.1	145	<0.05	< 5 × 10 ⁸
UGC 12510	E	NGC 7626	3542	—	—	15.8	210	<0.08	< 8 × 10 ⁸

⁽⁴⁾Optical radial velocity from NED

⁽⁵⁾Velocity centroid of HI line.

⁽⁶⁾Separation from targeted elliptical in arcmin

⁽⁷⁾Separation from targeted elliptical, assuming both systems lie at the distance given in Table 1

⁽⁸⁾Velocity width, calculated from intensity weighted velocity map, and with no correction for inclination.

^{(9)&(10)}6 σ limits, calculated from HI datacube smoothed to a velocity resolution of 42 km s⁻¹ and corrected for the primary beam attenuation.

^aIncludes all HI detections as well as limits for all galaxies with known redshifts found in NED that fall within the primary beam (15' radius) and velocity coverage of the VLA observations

^bUncataloged highly-inclined LSB companion at 11:21:51.5 +03:24:17 (J2000).

^cHI emission appears at the edge of the velocity coverage of the observations, so the high velocity range of the HI emission is not measured.

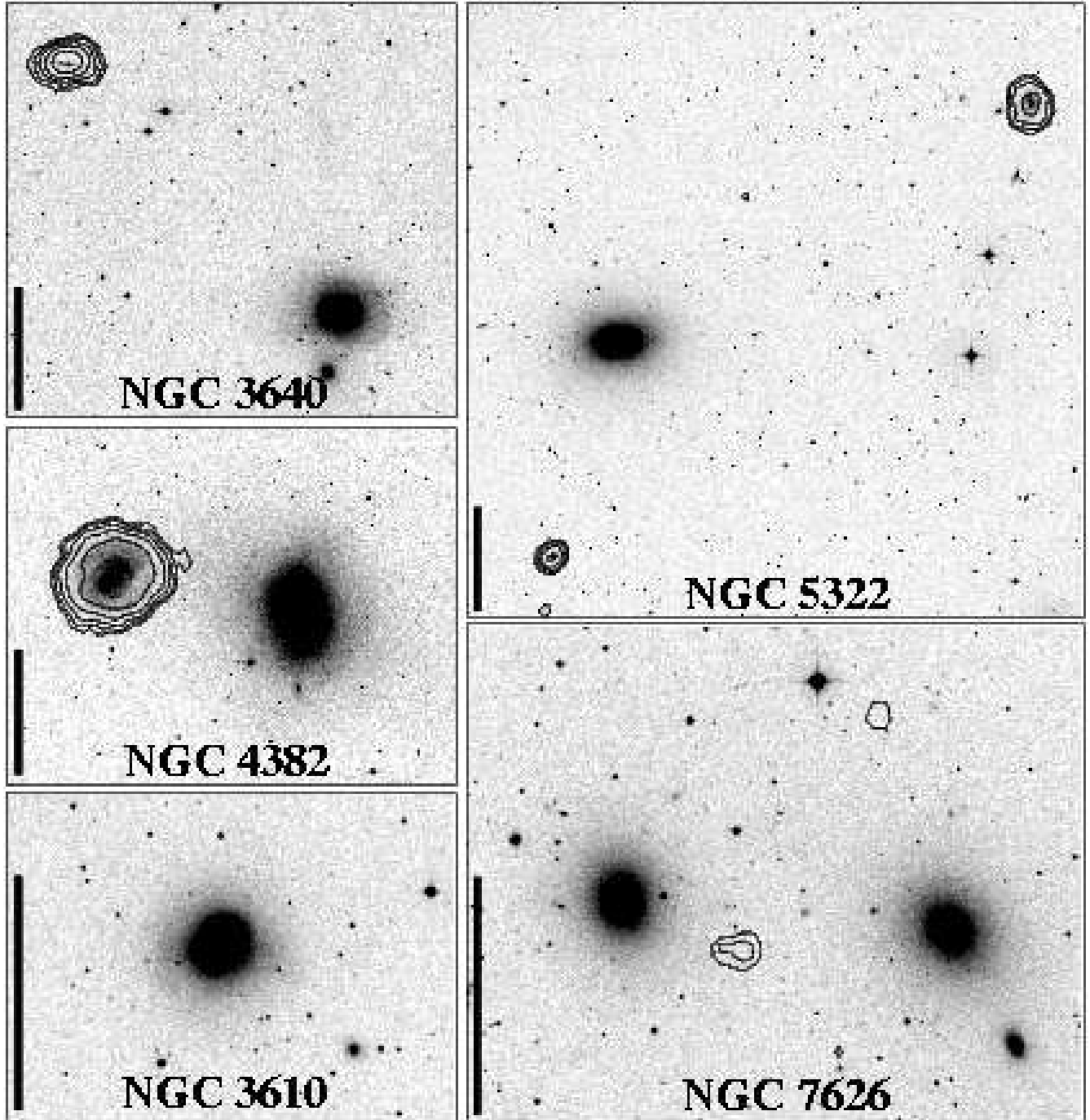


FIG. 1.— Montage of images for five E/SO galaxies with fine structure. Contours of HI column density are drawn upon a greyscale representation of the second generation blue Digital Sky Survey images. Image are oriented such that North is up and east is to the left. Clockwise from top left are the fields for NGC 3640, NGC 5322, NGC 7626, NGC 3610 and NGC 4382. Starting contours are drawn at levels of [27.6, 25.8, 24.4, 0.0, 24.5] Jy km s⁻¹ (respectively), which corresponds to an HI column density of 1×10^{19} cm⁻². Successive contours are drawn a factor of two higher. The vertical bar in each frame is 5' long. Of these five galaxies, only NGC 7626 has HI directly associated with the targeted elliptical (see Table 2). In these images HI is detected in: an uncataloged companion northeast of NGC 3640; MCG+10-20-039, a southern companion to NGC 5322; UGC 8714, a companion lying to the northwest of NGC 5322; a cloud lying west of NGC 7626; and NGC 4394 east of NGC 4382.

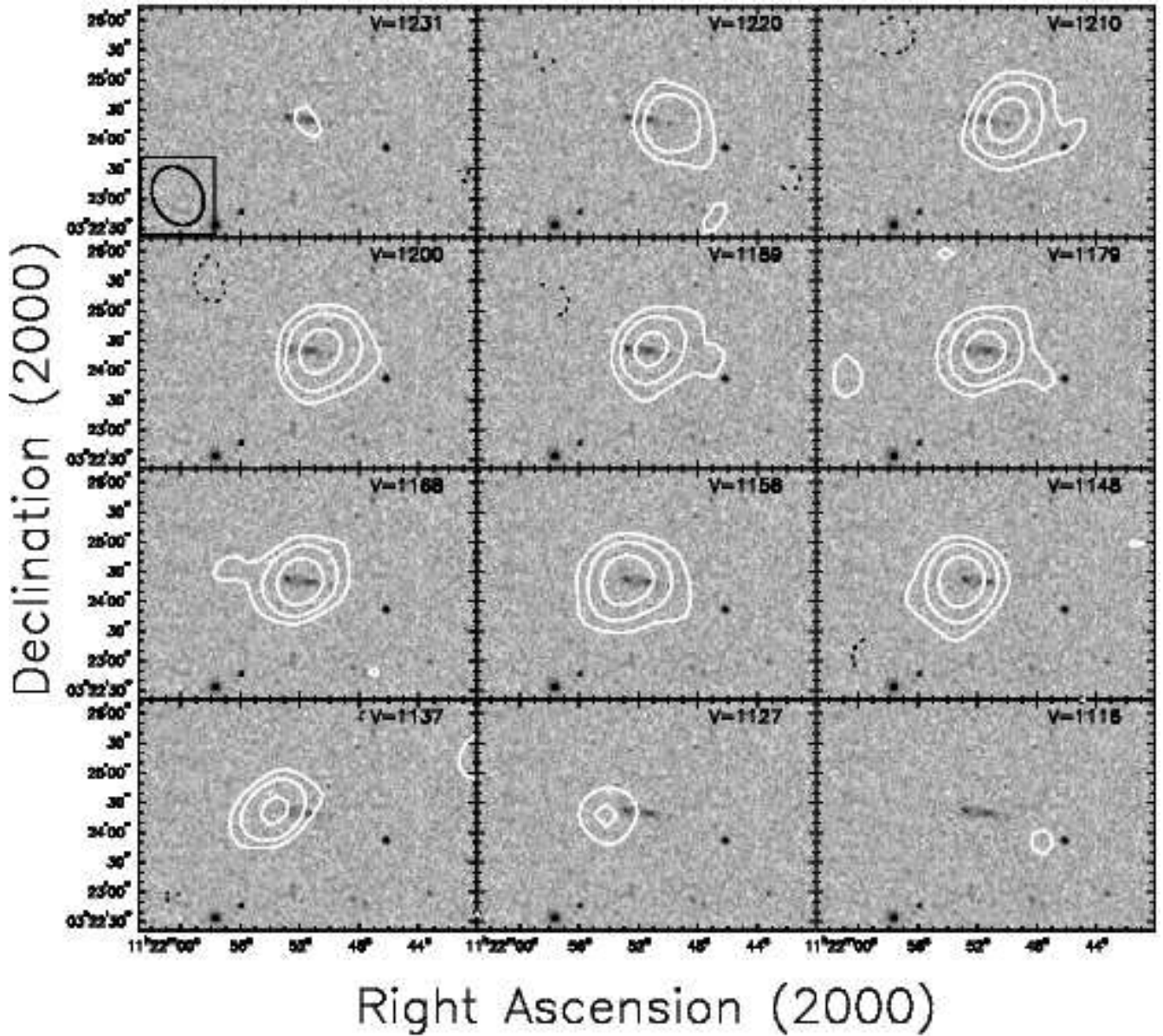


FIG. 2.— HI channel maps contoured upon a greyscale representation of the DSS optical image for the HI detected companion lying $15.1'$ (105 kpc) to northeast of NGC 3640, at $11:21:51.5 +03:24:17$ (J2000). The heliocentric velocity of each channel is given in the upper right of each panel, and the size of the synthesized beam ($62'' \times 49''$ FWHM) is indicated by the inscribed ellipse in the lower left corner of the first panel. Contours are drawn at levels of $[-3, 3, 6, 12] \times 1.2$ mJy beam $^{-1}$, where the lowest contour corresponds to an HI column density of 1.4×10^{19} cm $^{-2}$.

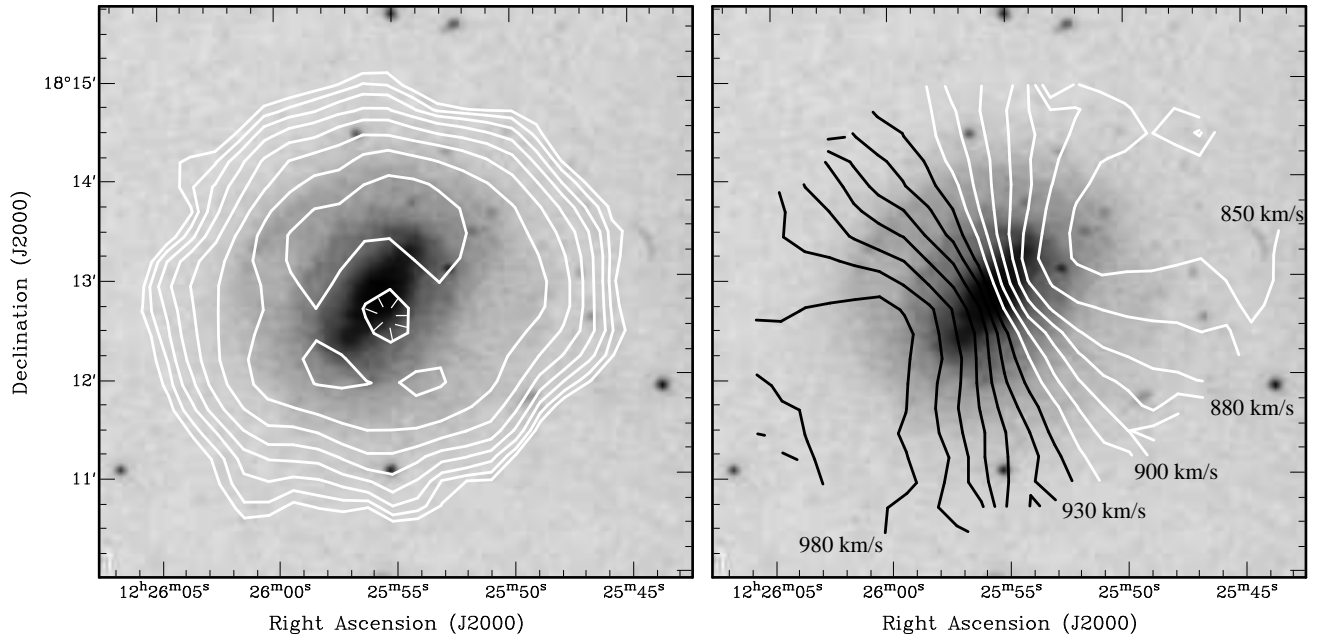


FIG. 3.— Integrated HI intensity (left) and intensity weighted isovelocity field (right) contoured upon a greyscale representation of the DSS optical image of NGC 4394, the barred companion east of NGC 4382. The integrated HI intensity is contoured at $48.9 \text{ Jy km s}^{-1} \times 2^{n/2}$, $[n=0,1,2,\dots]$, where the lowest contour corresponds to an HI column density of $2 \times 10^{20} \text{ cm}^{-2}$. The hatched contour represents a central depression in the HI distribution (see Fig. 4). The isovelocity field is contoured from 850–990 km s^{-1} in steps of 10 km s^{-1} , with white contours representing blue-shifted velocities relative to systemic, and black contours representing red-shifted velocities.

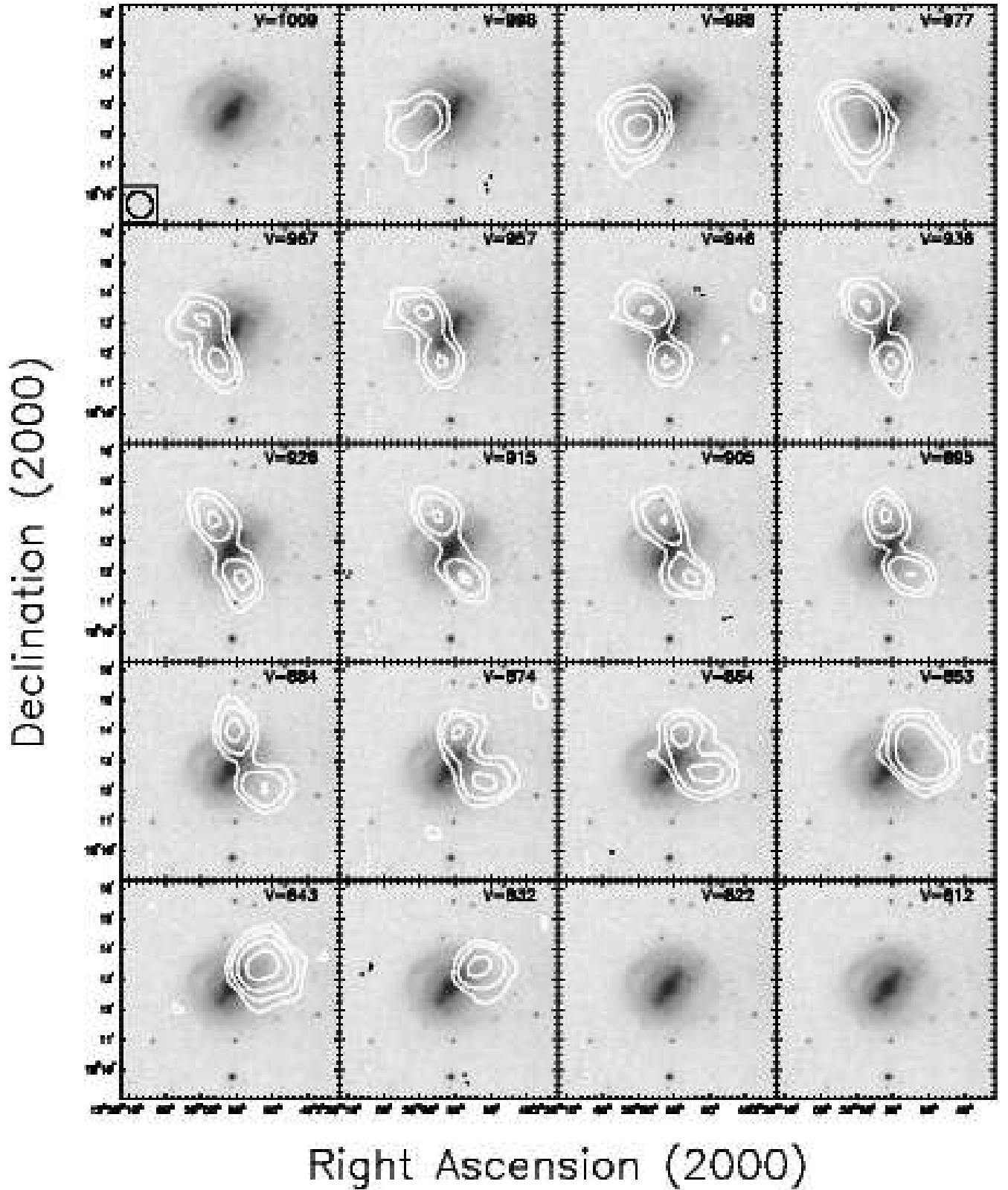


FIG. 4.— HI channel maps contoured upon a greyscale representation of the DSS optical image for NGC 4394, the barred companion lying $7.6'$ (37 kpc) to the east of NGC 4382. The heliocentric velocity of each channel is given in the upper right of each panel, and the size of the synthesized beam ($54'' \times 50''$ FWHM) is indicated by the inscribed ellipse in the lower left corner of the first panel. Contours are drawn at levels of $[-3, 3, 6, 12, 24] \times 0.76$ mJy beam $^{-1}$, where the lowest contour corresponds to an HI column density of 9.8×10^{18} cm $^{-2}$.

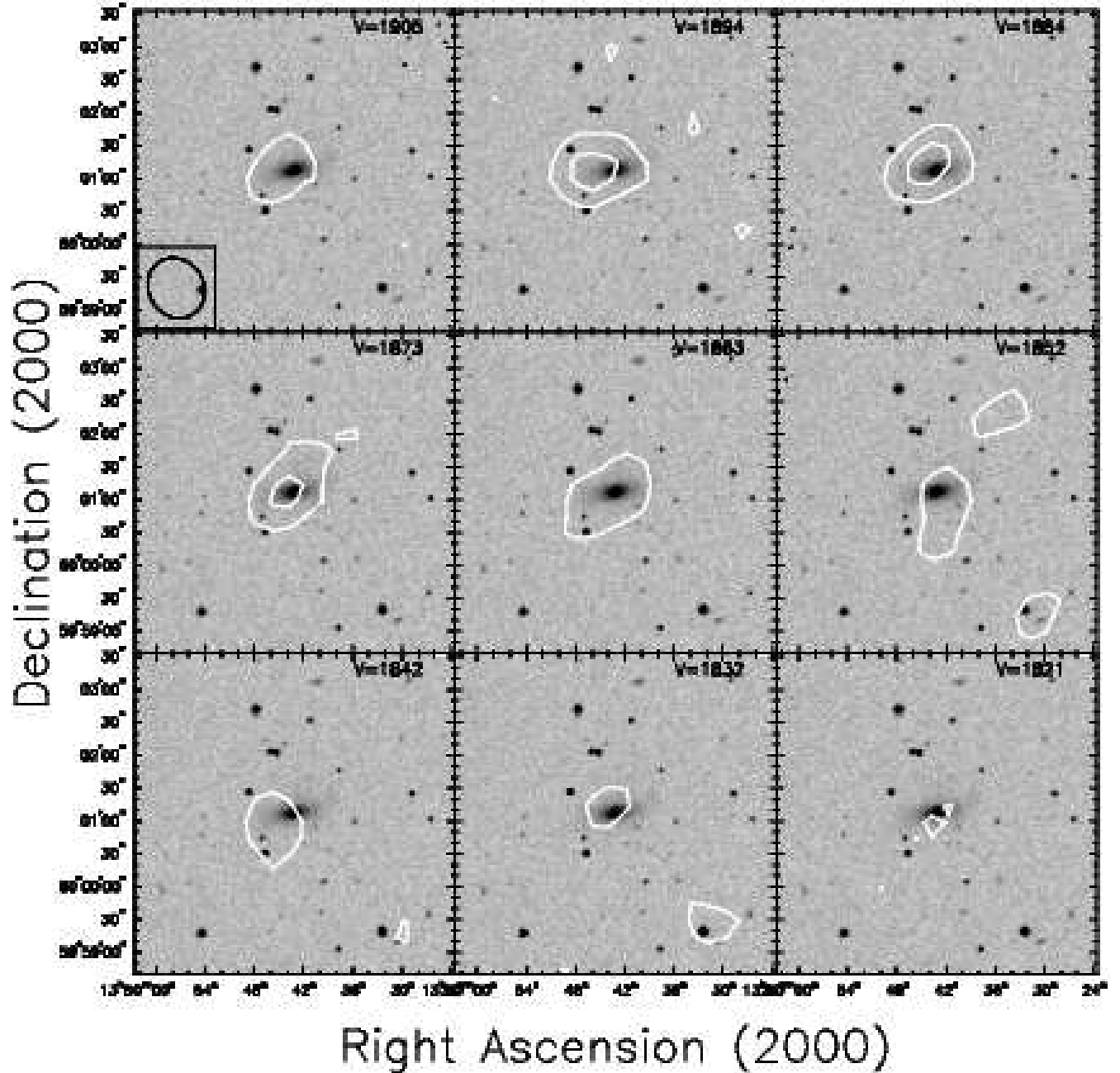


FIG. 5.— HI channel maps contoured upon a greyscale representation of the DSS optical image for MCG+10-20-039, the companion lying $10.9'$ (100 kpc) to the south of NGC 5322. The heliocentric velocity of each channel is given in the upper right of each panel, and the size of the synthesized beam ($57'' \times 50''$ FWHM) is indicated by the inscribed ellipse in the lower left corner of the first panel. Contours are drawn at levels of $[-3, 3, 6] \times 0.70$ mJy beam $^{-1}$, where the lowest contour corresponds to an HI column density of 8.5×10^{18} cm $^{-2}$.

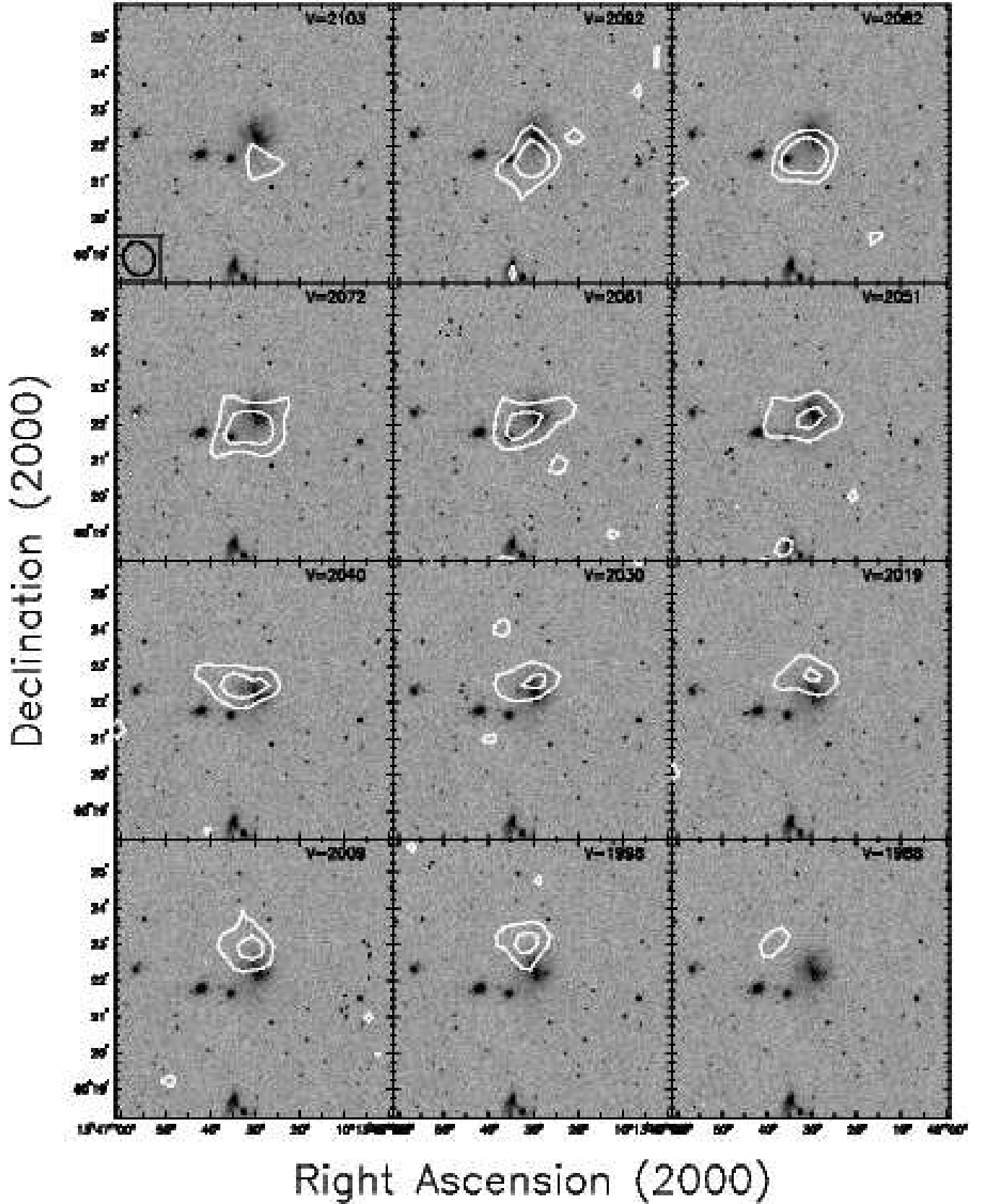


FIG. 6.— H I channel maps contoured upon a greyscale representation of the DSS optical image for UGC 8714, the companion lying $23.2'$ (215 kpc) to the northwest of NGC 5322. The heliocentric velocity of each channel is given in the upper right of each panel, and the size of the synthesized beam ($57'' \times 50''$ FWHM) is indicated by the inscribed ellipse in the lower left corner of the first panel. Contours are drawn at levels of $[-3, 3, 6] \times 2.9$ mJy beam $^{-1}$, where the lowest contour corresponds to an H I column density of 3.5×10^{19} cm $^{-2}$.

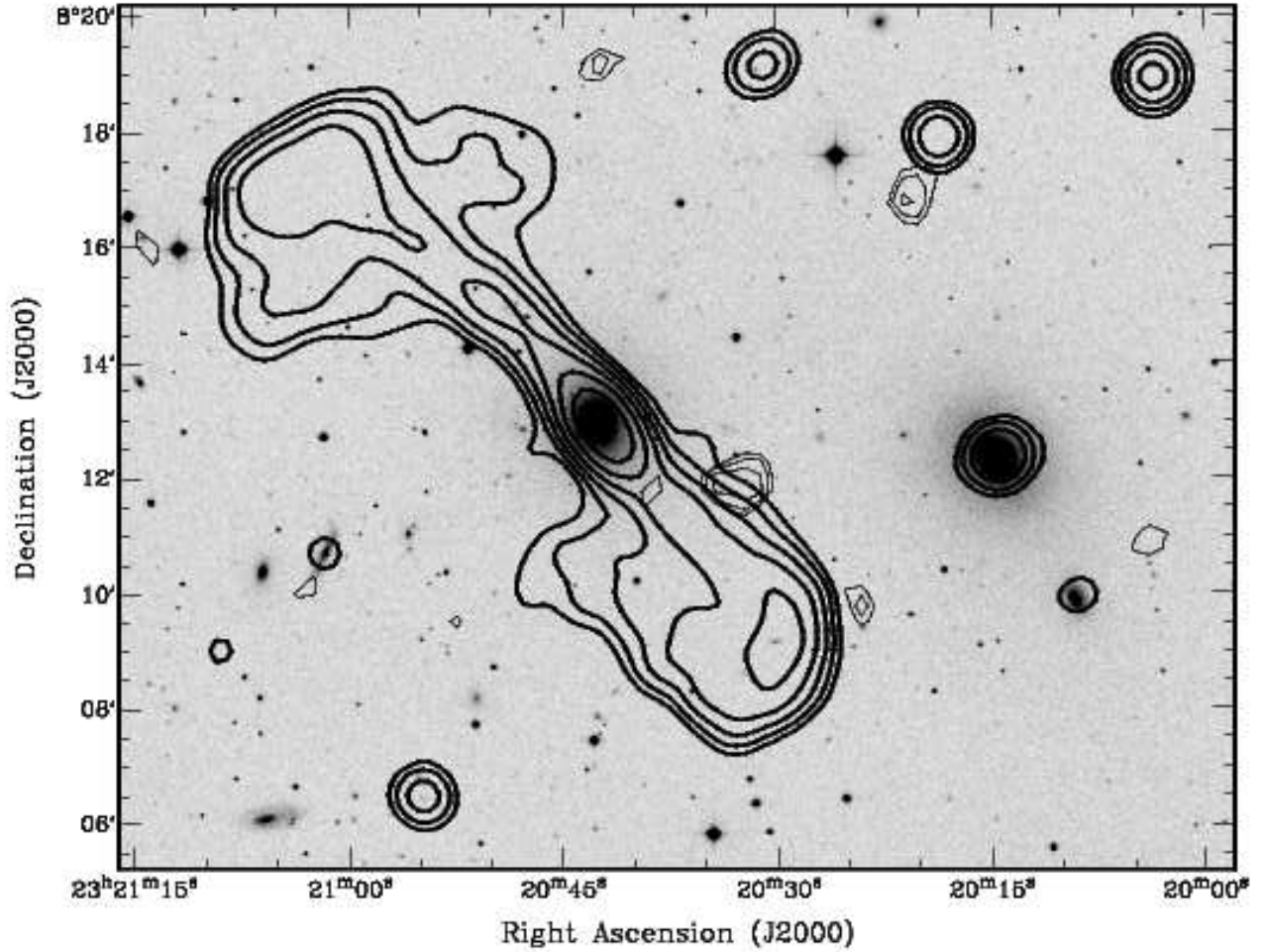


FIG. 7.— Radio continuum and HI emission in the NGC 7626 field. Thick contours show the distribution of the 1.4 GHz radio continuum. Contours start at 2 mJy beam^{-1} , with successive contours a factor of two higher than the previous contour. NGC 7619 lies directly to the west and is also a radio source, and NGC 7631 is the Sb galaxy lying directly to the east. Thin contours show the HI line emission integrated over the velocity range $3470\text{--}3600 \text{ km s}^{-1}$. Contours are drawn at levels of $[1, 2, 4] \times 10 \text{ mJy beam}^{-1} \text{ km s}^{-1}$, where the lowest contour corresponds to an HI column density of $4 \times 10^{18} \text{ cm}^{-2}$.

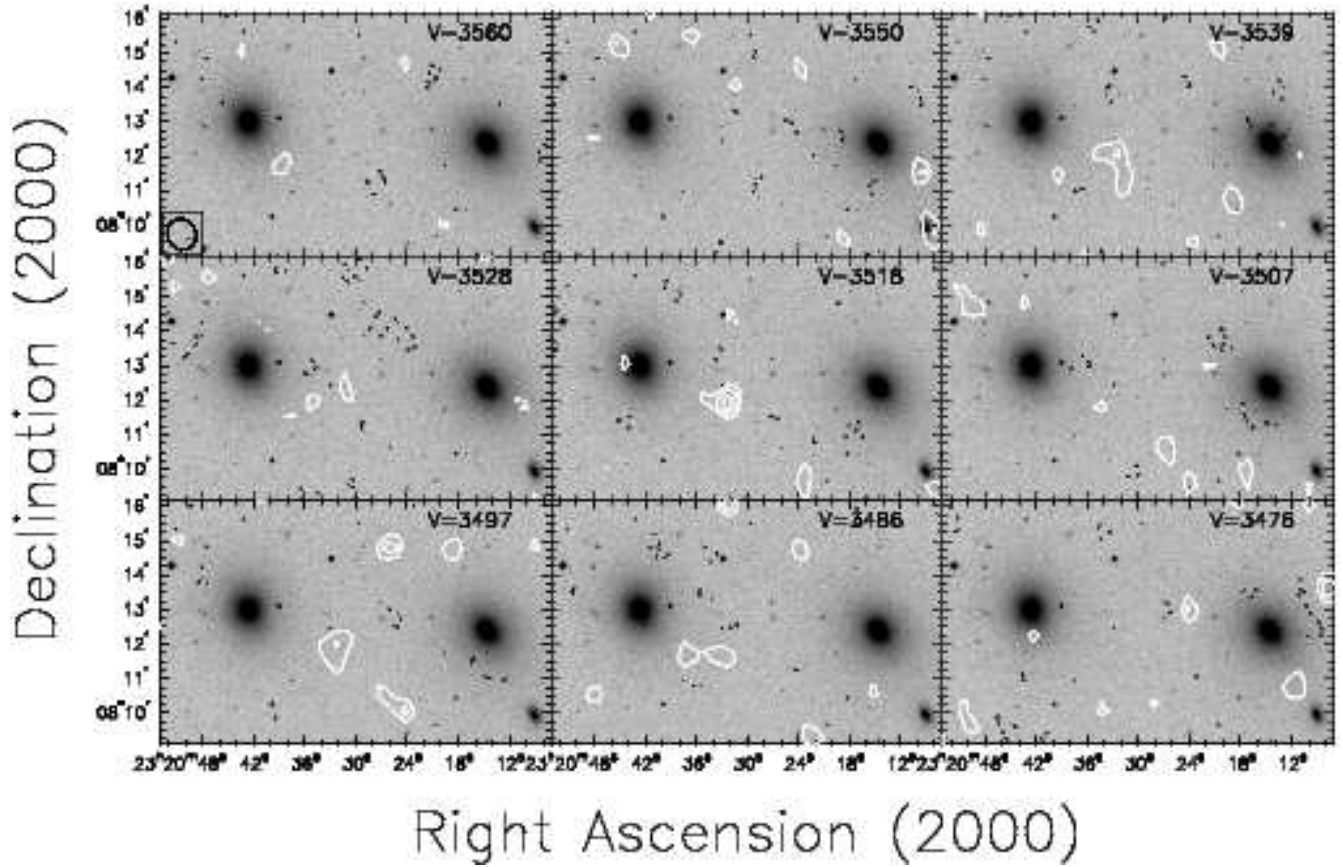


FIG. 8.— H I channel maps contoured upon optical image from the DSS for NGC 7626 (east) and NGC 7619 (west). The heliocentric velocity of each channel is given in the upper right of each panel, and the size of the synthesized beam ($55'' \times 49''$ FWHM) is indicated by the inscribed ellipse in the lower left corner of the first panel. Contours are drawn at levels of $[-3, -2, 2, 3, 4] \times 0.46 \text{ mJy beam}^{-1}$, where the lowest contour corresponds to an H I column density of $4 \times 10^{18} \text{ cm}^{-2}$.

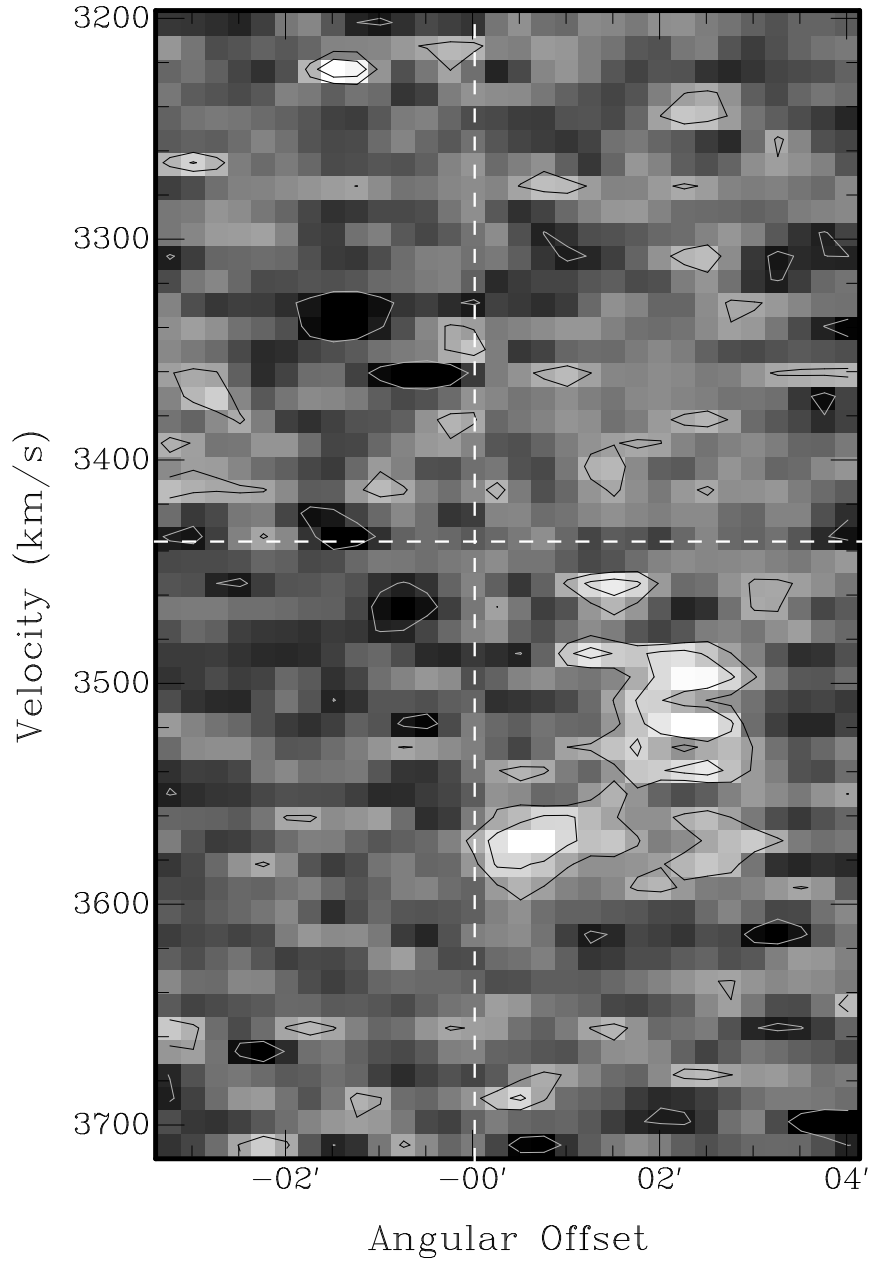


FIG. 9.— Position-Velocity plot through the peak in the HI emission in the NGC 7626 field. The position angle of the simulated “slit” is 90° (i.e., parallel to the right ascension axis), and centered at a declination of +08:11:42 (J2000). The right ascension and systemic velocity of NGC 7626 are indicated by vertical and horizontal dashed lines, respectively. Contours are drawn at $[-1, 1, 2] \times 0.46 \text{ mJy beam}^{-1}$.

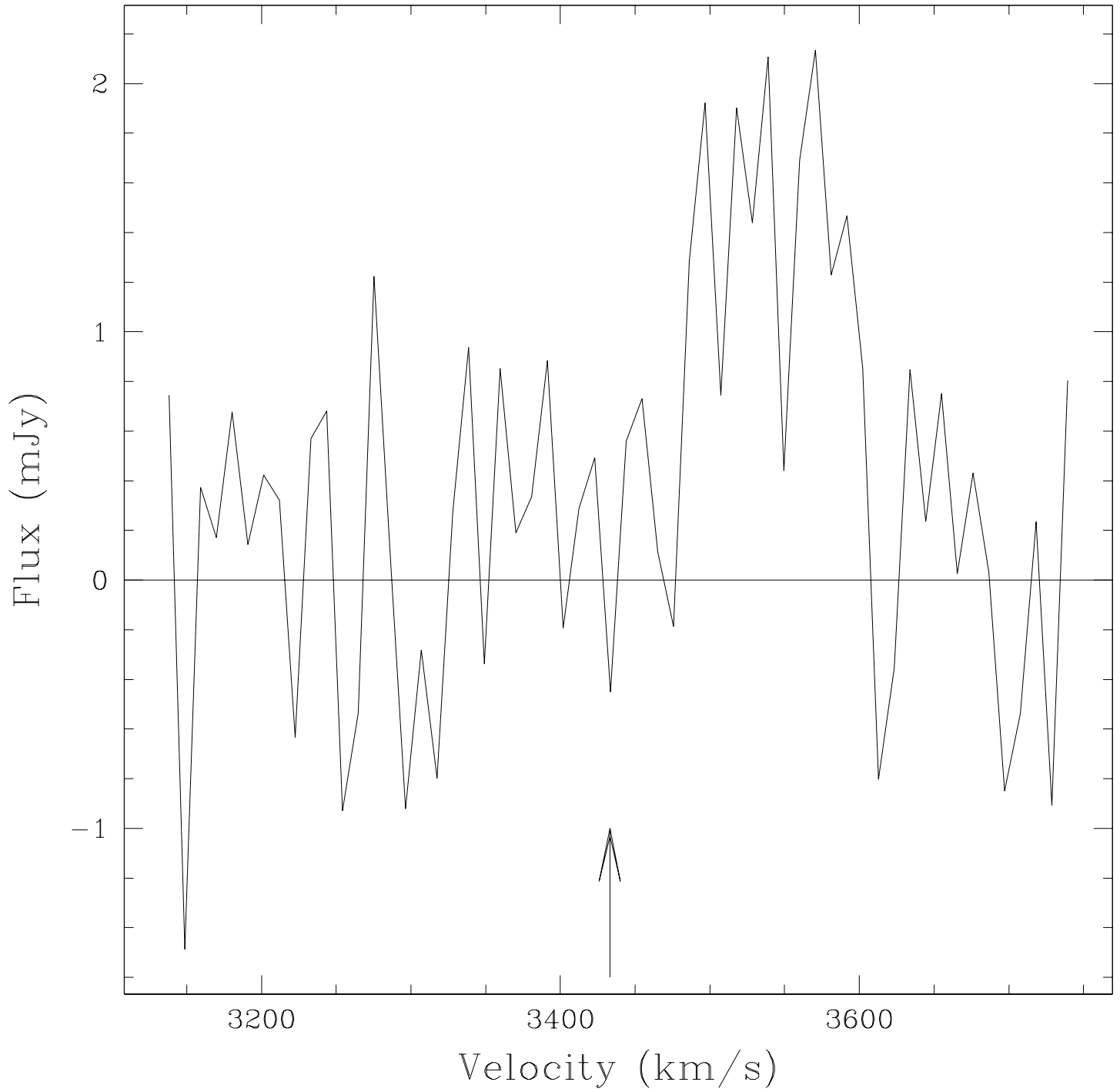


FIG. 10.— The integrated H I line profile extracted over the region containing the two H I features in the moment map. The velocity of NGC 7626 is indicated by the arrow.

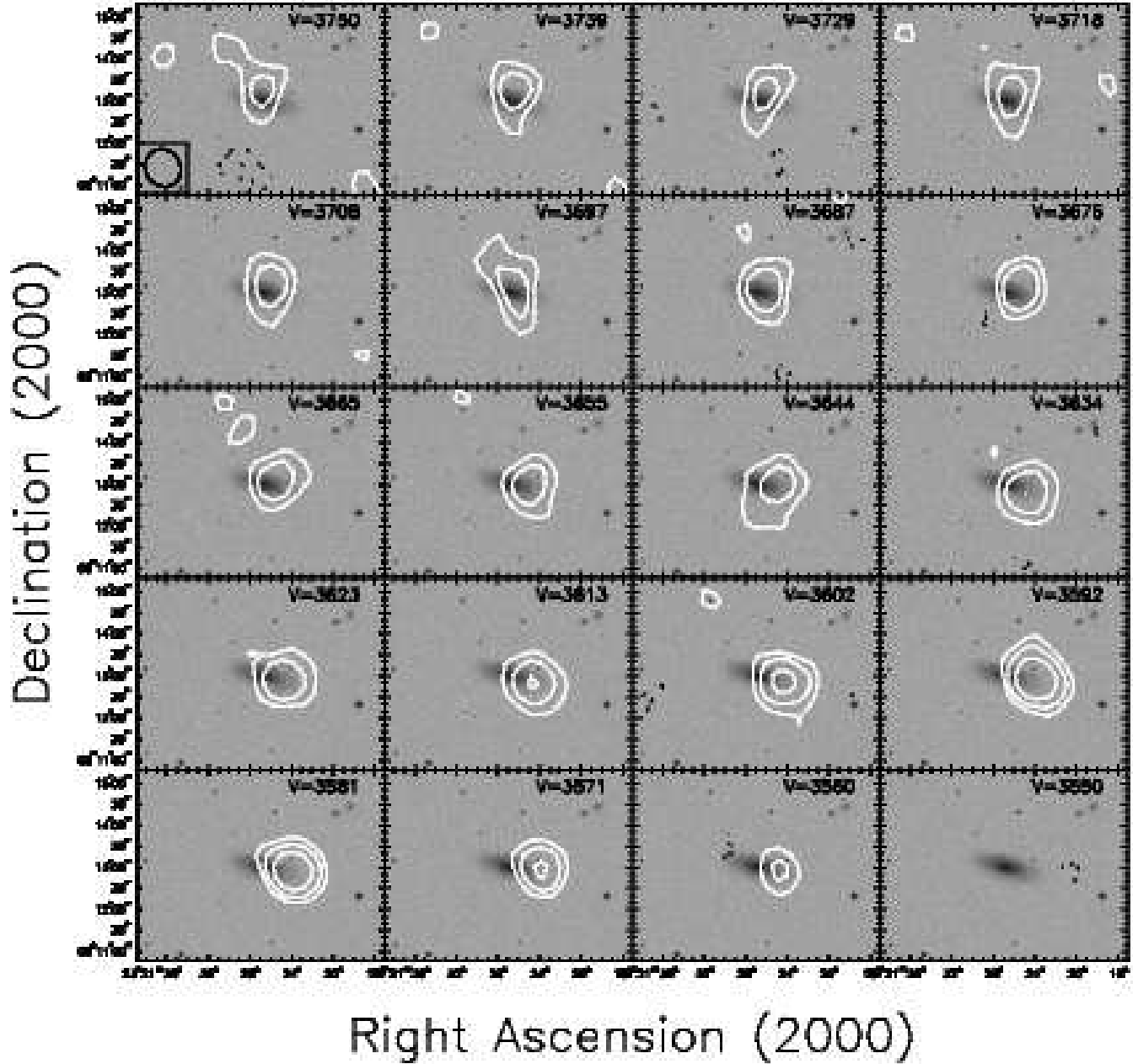


FIG. 11.— HI contours upon optical image from the DSS for HI channel maps contoured upon a greyscale representation of the DSS optical image for NGC 7631, the companion lying $11'$ (145 kpc) to the east to NGC 7626. The heliocentric velocity of each channel is given in the upper right of each panel, and the size of the synthesized beam ($55'' \times 49''$ FWHM) is indicated by the inscribed ellipse in the lower left corner of the first panel. Contours are drawn at levels of $[-3, 3, 6, 12] \times 0.64 \text{ mJy beam}^{-1}$, where the lowest contour corresponds to an HI column density of $8.2 \times 10^{18} \text{ cm}^{-2}$.

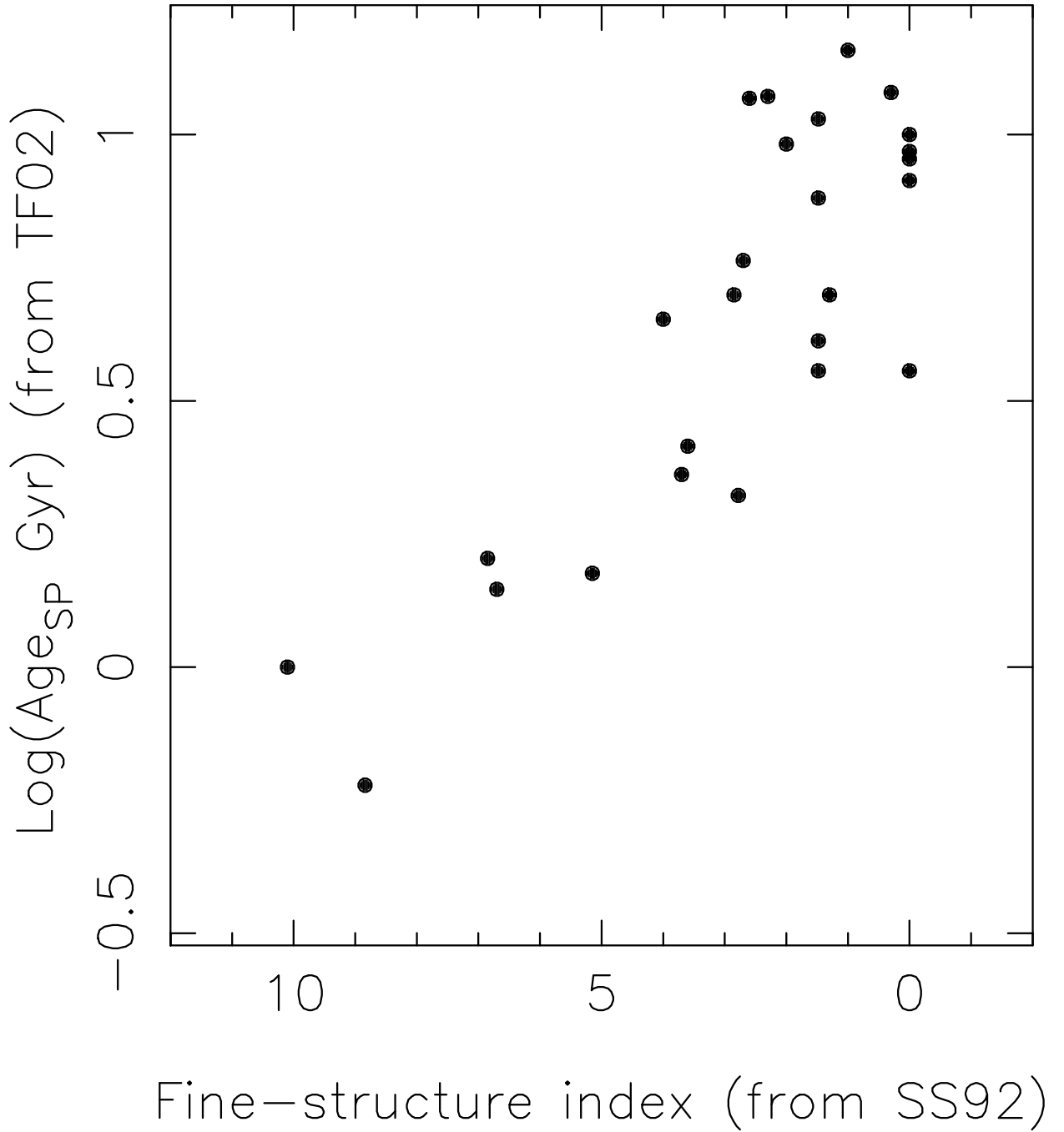


FIG. 12.— The logarithm of the spectroscopically determined age from TF02 (Age_{SP}), derived using SSP fits to H_{β} and $[MgFe]$ (combination of three) indices, versus the morphological fine-structure index from SS92 (Σ), for the 26 galaxies in common between the two samples.